JOTCS Journal of the Turkish Chemical Society Section: A Chemistry

TURKISH CHEMICAL SOCIETY

Revisiting Cu(II) Bound Amyloid-β40 and Amyloid-β42 Peptides: Varying Coordination Chemistries

Orkid Coskuner-Weber*

National Institute of Standards and Technology, Biochemical Reference Data Division, 100 Bureau Drive, Gaithersburg, Maryland 20899 USA, Turkish-German University, Molecular Biotechnology, Şahinkaya Caddesi No. 86, Beykoz, Istanbul 34820 Turkey, The University of Texas at San Antonio, Department of Chemistry, One UTSA Drive, San Antonio, Texas

Abstract: Metal ions and intrinsically disordered peptides amyloid-β40 and amyloid-β42 are at the center of Alzheimer´s disease pathology. Divalent copper ion binds to amyloid-β40 and amyloid-β42 peptides with varying coordination chemistries. Experiments face challenges in the measurements of divalent copper ion bound monomeric amyloid-β40 and amyloid-β42 in an aqueous solution medium because of fast conformational changes, rapid aggregation processes and solvent effects. Theoretical studies complement experiments and provide insights at the atomic and molecular levels with dynamics. However, until recently, potential functions for simulating divalent copper ion bound amyloid-β40 and amyloid-β42 peptides with varying coordination chemistries were lacking. Using new potential functions that were developed for divalent copper centers, Cu(II), including three histidine residues and an oxygen-ligated amino acid residue, the structures and thermodynamic properties of Cu(II)-bound amyloid-β40 and amyloid-β42 peptides in an aqueous solution medium were studied. For these purposes, extensive first principles calculations and replica exchange molecular dynamics simulations were conducted. In this study, the secondary and tertiary structural properties, conformational Gibbs free energy values, potential of mean force surfaces, salt bridges and aggregation propensities of aqueous Cu(II)-bound amyloid-β40 and amyloid-β42 peptides are presented. Different than previous findings in the literature, results clearly show that the coordination chemistry variations impact the structural and thermodynamic properties of divalent Cu(II) bound amyloid-β alloforms in water. Specificities about these differences are revealed in this study at the atomic level with dynamics. Results presented herein are the first to offer a comparison of the monomeric Cu(II)-bound amyloid-β40 and amyloid-β42 peptides with varying coordination chemistries using bonded model potential functions.

Keywords: Copper, amyloid-β, coordination chemistry, replica exchange molecular dynamics simulations, Alzheimer´s disease.

Submitted: May 16, 2018. **Accepted:** August 16, 2018.

Cite this: Coskuner-Weber O. Revisiting Cu(II) Bound Amyloid-β40 and Amyloid-β42 Peptides: Varying Coordination Chemistries. JOTCSA. 2018; 5(3): 981-1008.

DOI: http://dx.doi.org/10.18596/jotcsa.424144.

***Corresponding author.** E-mail: weber@tau.edu.tr.

INTRODUCTION

Divalent copper ion impact on the aggregation rate of amyloid-β alloforms Aβ40 and Aβ42 is debated in the literature (1). Based on the solution pH, Cu(II) concentration, and the type of fibrillar or amorphous state monitored, both an increase and a decrease of Aβ aggregation have been shown (1-4). A few investigations reported that Cu(II) does not promote aggregation of Aβ (3, 5). On the other hand, several studies show that Cu(II) binding increases non-fibrillar, or amorphous, aggregation of Aβ, especially at low pH (6.6) and physiologically relevant concentrations of Cu(II) (2, 4, 6-16). Additionally, some research studies reported an

increase in oligomer formation while others presented the vice versa (6, 17). Nevertheless, Karr *et al.* reported the formation of fibrillar aggregates for Cu(II)-bound Aβ (18, 19). Moreover, some research groups presented that fibrillar aggregation of Aβ is promoted by Cu(II) at sub-equimolar Cu(II) concentrations, however, amorphous aggregation and spherical oligomer formation of Aβ is enhanced at supra-equimolar concentrations of Cu(II) (11, 20-22). The toxicity of Cu(II)-bound Aβ [Cu(II):Aβ] is also debated in the literature. Both protective and toxic effects have been reported for Cu(II):Aβ (1, 10, 23-27). Many studies report that Cu(II)-binding enhances the neurotoxicity of Aβ (8, 28). However, there are studies that report decreased neurotoxicity of Cu:Aβ in comparison to free Aβ (10, 29). Interestingly, a few studies have presented that Cu:Aβ exhibits significant neurotoxicity at sub-equimolar concentrations that is lost at super-equimolar concentrations (11, 30). Understanding the impact of Cu(II) binding on Aβ structures could aid in deciphering the role of divalent transition metal ions towards aggregation and toxicity in Alzheimer´s disease (AD) pathology. Cu(II) binding impact on the monomeric structures of Aβ including variations between the Aβ40 and Aβ42 alloforms has not yet reached a consensus.

Cu(II) and Aβ coordination chemistry is greatly debated in the literature (18, 19, 31-52). In general, the coordination chemistry of Cu(II) with Aβ is reported to exist as two separate species transition between each other depending on the pH. Species I occurs at low pH values while species II exists at high pH values with the transition between these two species occurring at pH 8 ± 1 (18, 33, 36, 42, 47, 49). The species I structure is proposed to be dominant at physiologically relevant pH. 3N1O coordination mode that is generally agreed upon was presented using extended X-ray absorption fine structure (EXAFS) and electron paramagnetic resonance (EPR) spectroscopies (1). Two main hypotheses regarding the identity of the nitrogen ligands are found in the literature: either three His amino acid residues (His6, His13 and His14) or two His amino acid residues and the N-terminus. Strong evidence for the three His residues coordination mode has been provided by EXAFS, CD and NMR measurements while the two His and N-terminus coordination mode is supported prominently by EPR measurements (1, 9, 33, 36, 41, 42, 45, 54). However, it is important to note that it is possible for both coordination mechanisms to occur due to the intrinsically disordered nature of Aβ (1). Several different candidates for a possible oxygen ligand in the Cu:Aβ metal-ligand sphere have also been proposed (1). Specifically, Glu3, Glu11, the carboxylate group of Asp1, a backbone carbonyl oxygen atom or the phenolate group of Tyr10 have each been presented as a potential Cu(II) coordination ligand in Aβ (1). Out of these potential coordination ligands, Asp1 and Tyr10 have been the most heavily implicated (18, 33, 36, 41). The Asp1 ligand is implicated from EPR measurements of D1N mutant-type and wild-type Aβ that present a modified EPR spectrum upon mutation (18). Despite, Tyr10 is supported by Raman and UV-visible spectroscopies, EXAFS measurements, and EPR studies of Y10A mutant-type Aβ42 with Cu(II) (33, 46-48, 55). Furthermore, Glu3 and water were eliminated as potential ligands based on an EPR study of E3Q Aβ16 and 17O-labelled H_2O (18, 33, 41). We should mention here that several studies including our own have shown that the mutation of a single residue of Aβ significantly alters the conformational ensemble of Aβ, which in turn might affect potential coordination sites differently than wild-type Aβ (56, 57).

Quantum mechanical (QM) techniques can provide valuable information but full-length structure of the transition metal ion-bound proteins cannot be studied using QM (50, 59-72). Therefore, active site truncated models are widely utilized. QM and molecular mechanics (MM) techniques (QM/MM) have also been utilized for investigating metalloproteins (73-83). Resulting simulation accuracies can be influenced by the time scale difference between the QM and MM regions, the treatment and location QM and MM regions boundary, and conformational sampling limitations without using special sampling techniques for enhancing the conformational sampling. Advancement of QM/MM to overcome these disadvantages is currently ongoing in various research groups. MM is the most commonly used technique for investigating the chemical and physical properties of full-length metalloproteins. However, many required force field parameters for the metalloproteins do not exist in the scientific literature. In a previous investigation, first principles calculations to optimize different divalent Cu coordination complexes that contain full-length residues were used: three His residues and a different fourth binding ligand (aspartic acid, tyrosine, or glutamic acid); Cu:His_3Asp, Cu(II):His_3Tyr, and Cu:His_3Glu (84). We developed the missing potential functions for Cu:His_3Asp, Cu:His_3Glu, and Cu:His_3Tyr (84). Using the potential functions for Cu:His_3Glu, the structures and thermodynamic properties of Cu:His_3Glu bound Cu(II):Aβ40 and Cu(II):Aβ42 in an aqueous solution environment using a continuum model for water were studied (85). Recent studies using an explicit model for water show that the confined aqueous volume has a significant impact on the structural and thermodynamic properties of the full-length Aβ peptide (86). In addition, there are studies that report the physical, biological and chemical characteristics of Cu(II):Aβ utilizing smaller fragments instead of using full-length metalloproteins (87). Such investigations are questionable in computing the properties of full-length disordered metalloproteins. Specifically, the fragment size affects the determined Aβ structures in water (88). In addition, Zn(II) force

field parameters were utilized in a few Cu:Aβ investigations because parameters for Cu(II) lacked before we developed those (see, for example, 89). Zn(II) and Cu(II) have varying number of electrons and coordination chemistry specificities; Jahn-Teller effects cannot be ignored. Strodel and co-workers developed a nonbonded model Cu(II) model that includes Jahn-Teller effects (56). However, recent investigations showed that the charge transfer effects and electrostatic charges and between the transition metal ion and biospecies dominate the determined biometallic structures (90-93). Development of force field parameters occurs using nonbonded or bonded models. Full ionic charge without charge transfer is used in nonbonded models. Previous MM studies used Zn(II) potential functions for Cu(II) simulations utilizing a bonded model. We develop the bonded model for potential functions in our studies (84). Kodali *et al.* showed that β-sheet conformation plays a key role in Aβ fibril formation mechanisms (94). NMR measurements presented parallel β-sheet structure within protofilaments (95). The vicinity of Ile41 and Ala42 provides a difference between the primary strutures of Aβ40 and Aβ42. Central hydrophobic core (Leu17-Ala21), turn region (Val24-Asp27) and second hydrophobic region (Gly29-Met35) play central roles in Aβ aggregation (56, 85, 96). Metal:Aβ structures have been investigated heavily using NMR, Fourier transform infrared spectroscopy and X-ray absorption spectroscopy (97-101). Hane *et al.* illustrated that the reactivity of the Aβ peptide increases upon Cu(II) coordination (102). Higher dimerization tendencies upon Cu(II) coordination, which presented that Cu:Aβ becomes more reactive toward Aβ were shown. Additionally, Nair *et al.* showed larger binding affinity values for Cu(II):Aβ than for Zn(II):Aβ, indicating stabilized Aβ aggregation processes with Cu(II) coordination (103). Moreover, Liao et al. studied the conformational transitions of the amyloid-β42 peptide upon Cu(II) binding and pH changes using Hamiltonian-REMD simulations and via utilizing the binding of Cu(II) to Asp and His residues. They reported that Cu(II) binding and a low pH-mimicking acidosis, linked to inflammatory processes in vivo, accelerate the formation of β-strands in Aβ42 and lead to the stabilization of salt bridges that was previously shown to promote Aβ aggregation. Their results illustrated that Cu(II) binding and mild acidic conditions can shift the conformational equilibrium towards aggregation-prone conformers for the monomeric Aβ42 (57). In an additional study, Strodel and co-workers reported the conformational changes of the Aβ42 dimer upon Cu(II) coordination using the Asp and His coordination nodes via conducting H-REMD simulations (58). They showed that Cu(II) binding, oxidation and a decrease in pH are relevant to the oligomerization of Aβ42. An increased β-sheet content was reported upon Cu(II) binding.

Experiments face challenges in the measurements of Cu:Aβ monomers and oligomers due to rapid aggregation processes, fast conformational changes and solvent effects. Theoretical studies complement experiments and give detailed knowledge that are otherwise challenging to obtain utilizing conventional techniques. Here, we investigated the chemical and physical characteristics of Cu(II):Aβ40 and Cu(II):Aβ42 utilizing the Cu(II):His_3Asp and Cu(II):His_3Tyr coordination spheres and our new potential functions for these organometallic centers. We simulate and compare the structural and thermodynamic properties of Cu(II):Aβ alloforms utilizing the Cu(II):His_3Asp and Cu(II):His_3Tyr coordination spheres to those of Aβ and Cu(II):Aβ along with the Cu(II):His_3Glu coordination sphere. For these purposes, the structural and thermodynamic properties were investigated dynamically at the atomic level. To the best of our knowledge, this study represents the first investigation of Cu(II)-bound Aβ40 and Cu(II)-bound Aβ42 alloforms´conformational changes with varying coordination chemistries using a bonded model for the Cu(II) ion.

Aβ40/Aβ42: DAEFRHRSGYEVHHQKLVFFAEDVGSNKGAIIGLMVGGVV(I)(A)
Scheme 1. Primary structure of Aβ40 and Aβ42.

MATERIALS AND METHODS

Ab Initio Quantum Chemical Studies: First principles calculations were performed using the Becke, 3-parameter, Lee-Yang-6 Parr (B3LYP) hybrid functional utilizing the 6-31G*, 6-31G**, cc-pVDZ, ahlrichs-vdz, ahlrichs-vtz, def2-svpd, def2-tzvp and lanl2dz-ecp basis sets in extensive separate sets of calculations (104). In order to determine the structural properties and binding affinities as well as the impact of the chosen basis set on the Cu(II):His_3(H_2O), Cu(II):His_3Tyr, Cu(II):His_3Asp and Cu(II):His_3Glu organometallic complexes, we performed separate sets of first principles calculations. We optimized the structures of Cu(II):His_3(H_2O), Cu(II):His_3Tyr, Cu(II):His_3Asp, Cu(II):His_3Glu, H_2O, Asp, Tyr, Glu and Cu(II):His_3 to estimate the binding affinities of H_2O, Asp, Glu and Tyr with the same receptor; Cu(II):His_3 using different basis sets for gaining insights into the impact of the chosen basis set on the predicted structures and energetics.

Replica Exchange Molecular Dynamics Simulations: To simulate the Cu(II):Aβ40 and Cu(II):Aβ42 alloforms using varying coordination chemistries; Cu(II):His_3Asp and

Cu(II):His_3Tyr coordination chemistries through a bonded model for the metal-ligand moiety, which embraces electrostatic interactions, the potential functions for the distorted square planar Cu(II):His_3Asp and Cu(II):His_3Tyr moieties utilizing full-size metal-ligand complexes and extensive first principles calculations were developed (84). These first principles calculations were validated by experiments and initial structures were generated using first principles calculations (84). Initial Cu(II):His_3Asp and Cu(II):His_3Tyr structures from first principles to the full-length Aβ40 and Aβ42 peptides´ residues were connected. REMD simulations were conducted utilizing these potential functions for the metal-ligand moities along with the Amber ff99SB parameters for the protein with which the potential functions are compatible with (84, 105-107). Furthermore, same parameters for the wild-type Aβ40, Aβ42, Zn(II):Aβ40, Zn(II):Aβ42, Cu(II):Aβ40 and Cu(II):Aβ42 with the Cu(II):His_3Glu coordination sphere were used before and the usage of the same sets of parameters is required for more accurate comparison reasons with these species (85, 88, 107). Additional simulations using the Amber ff14SB parameters and the TIP5P model for water were conducted (Supplementary information section; Fig. S1A and Fig. S1B). The correlations between Cα and Hα chemical shift values for the Aβ42 peptide in aqueous solution utilizing the structures from our simulations and experimental chemical shift values provided by Dr. Michael Zagorski (CWRU) are presented in Fig. S2A and Fig. S2B (supplementary information). Following previous investigations for comparison reasons, the Onufriev-Bashford-Case generalized Born implicit solvent model was used along with the particle mesh Ewald summation method with a cut-off value of 25 Å (105-108 and references therein). Langevin dynamics with a collision factor of 2 ps^{-1} was used to control the temperature (107). Structures were first equilibrated for 500 ps for each replica and trajectories were saved for every 500 steps. The integration time step for each replica was 2 fs. Exchange attempt time interval between different replicas was set to 5 ps and 16 replicas were used with exponentially distributed temperatures between 280 K and 408 K (56, 88, 96, 104, 108, 109). The production total time was 51.2 μs. To test the convergence, time-dependent secondary structure component abundances were used (see the supplementary information section; Fig. S3A and Fig. S3B). Results presented that the systems require 60 ns of the simulation time to converge, which is in agreement with previous studies (56, 85, 88, 96, 108-110). Physiological temperature results are reported.

We should mention here that simulations using an implicit model for water for overcoming the confined aqueous density effects do not embrace intermolecular hydrogen bonding interactions between the metallopeptides and the solvent molecules. Specific heat value for pure liquid water does not remain constant in parallel tempering replica exchange molecular dynamics simulations (111). Most recently, we showed that the secondary and tertiary structures as well as the thermodynamic properties of Aβ40 and Aβ42 are affected by the confined aqueous volume effects using an explicit model for water (86). Nevertheless, we also investigated the influences of intermolecular interactions between solute and solvent using our own explicit model for water (modified TIP5P) (109). These studies showed that the structural properties are affected by the usage of implicit/explicit water models. Thermodynamic trends are not affected by the usage of implicit or explicit water models. Following recent studies, the thermodynamic properties were investigated using the molecular mechanics/Poisson-Boltzmann surface area method and potential of mean force surfaces (83, 85, 86, 88, 96, 108-112). For the potential of mean force (PMF) surfaces, the coordinates of the end-to-end distances were used along with the radius of gyration values (56, 83, 85, 96, 108, 109). The software DSSP was used for predicting the secondary structure components and their abundances (56, 83, 85, 96, 108, 109, 113). Intra-molecular interactions exist when the two centers of mass of two residues are within a distance of 9.0 Å. Furthermore, a hydrogen bond exists when the same distance between the donor hydrogen atom and acceptor atom is less than or equals to 2.5 Å along with a criteria for the hydrogen bond angle (≥ 113°) (56, 83, 85, 96, 108, 109). A salt bridge exists between hydrogen bonded atoms with opposite electrostatic charges. The method developed by Pawar et al. for calculating the intrinsic aggregation propensities of individual amino acids was utilized (114).

RESULTS AND DISCUSSION

Figure 1 shows the optimized structures of the Cu(II):$His_3(H_2O)$, Cu(II):His_3Tyr, Cu(II):His_3Asp and Cu(II):His_3Glu complexes at the DFT level.

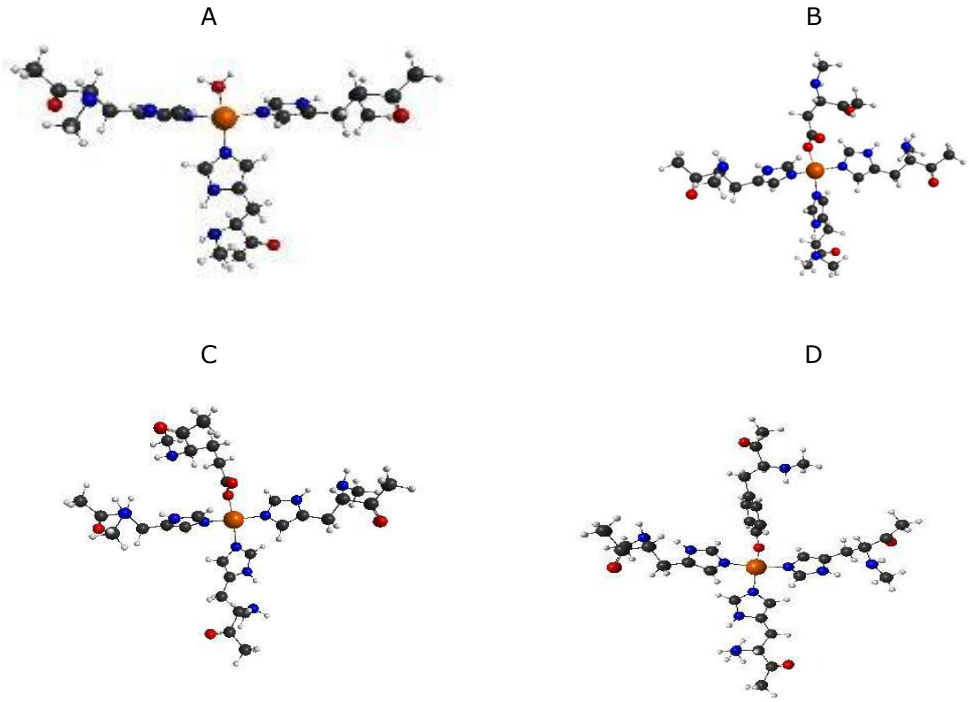

Figure 1. Optimized structures of (A) Cu(II):His_3(H2O), (B) Cu(II):His_3Asp, (C) Cu(II):His_3Glu and (D) Cu(II):His_3Tyr using the B3LYP functional along with the def2-tzvp basis set.

Figures S4 and S5 in the supplementary information section present the calculated bond distances - using varying basis sets - between Cu(II) and coordinating N and O atoms. Figure S6 in the supplementary information section depicts the optimized bond angles between coordinating residue atoms and Cu(II). Tables 1-4 present the total energies and binding energies for Cu(II):$His_3(H_2O)$, Cu(II):His_3Tyr, Cu(II):His_3Asp and Cu(II):His_3Glu using all basis sets at the B3LYP level of theory. As expected, the smallest energy is obtained utilizing the def2-tzvp basis set for Cu(II):$His_3(H_2O)$, Cu(II):His_3Tyr, Cu(II):His_3Asp and Cu(II):His_3Glu. Cu(II):His_3Tyr is energetically the most stable structure (-3930.6288 H) while Cu(II):$His_3(H_2O)$ possesses the largest energy with a value of -3373.7600 H utilizing the def2-tzvp basis set. The order in stability follows: Cu(II):His_3Tyr > Cu(II):His_3Glu > Cu(II):His_3Asp > Cu(II):$His_3(H_2O)$. Overall, the calculated binding energies of the Asp, Glu, Tyr and H_2O show that these bindings to the Cu(II):His_3 complex is preferred. The order of binding energies from the largest negative to the smallest negative value is (Tables 1-4): Asp > Glu > Tyr > H_2O. The same trend was obtained by Mantri *et al.* for Asp, Glu and Tyr residues (139). Cu(II):$His_3(H_2O)$ has 14 heteroatoms, Cu(II):His_3Tyr possesses 17 heteroatoms while Cu(II):His_3Glu and Cu(II):His_3Asp each have 16 heteroatoms. Quantum chemical energetics is not related to the number of heteroatoms and yields usually large amount of total energies as expected. For instance, Xu *et al.* calculated the binding energy using the B3LYP/6-31G(d) level of theory between Cu(II) and of different conformations of a smaller fragment Aβ16 and reported binding energies that vary between -911.73 kcal/mol and -415.78 kcal/mol (87). MacKerell and co-workers reported about 10 kcal/mol energy difference just for the anti and syn conformations of deoxyribonucleosides (138). Moreover, Rickard et al. calculated the binding affinities for model biologically available potential Cu(II) ligands relevant to Alzheimer´s disease using smaller models and the B3LYP/6-31G(d) level of theory utilizing the COSMO model for water and their energetics shows that the addition of one water molecule to a much smaller model compound namely Cu(II):$(H_2O)_3$ has an enthalpy change of 170.8 kJ/mol (68). Furthermore, Mantri *et al*. reported binding Gibbs free energies that vary between -45.34 kcal/mol and -95.06 kcal/mol for small model comlexes representing Asp, Glu, Ser and Tyr binding to Cu(II):His_3 (139) using the B3LYP/6-31G** level of theory. However, we should note that these calculations were conducted in the gas phase or using a continuum model for water at the electronic level and these results might change with the inclusion of explicit water molecules.

Table 1. The total energies calculated for Cu(II):His_3(H2O), Cu(II):His_3 and H_2O using the optimized structures with each basis set and through performing single point energy calculations on Cu(II):His_3 and on water. The binding energy of water was calculated as well.

Basis Set	Cu(II):His_3(H_2O) Total Energy (Hartree)	Cu(II):His_3 Total Energy (Hartree)	H_2O Total Energy (Hartree)	Binding Energy (kcal mol^{-1})
6-31G*	-3372,8092	-3296,3527	-76,4086	-30,04
6-31G**	-3372,8886	-3296,4214	-76,4194	-29,98
cc-pVDZ	-3373,2398	-3296,7751	-76,4215	-27,13
Ahlrichs-VDZ	-3370,9786	-3294,6068	-76,3202	-32,41
Ahlrichs-VTZ	-3373,0694	-3296,5641	-76,4303	-47,07
Def2-SVPD	-3371,7909	-3295,3767	-76,3817	-20,43
Def2-TZVP	-3373,7600	-3297,2626	-76,4635	-21,32
LANL2DZ-ECP	-1928,3955	-1851,9338	-76,4141	-29,84

Table 2. The total energies calculated for Cu(II):His_3Asp, Cu(II):His_3 and Asp using the optimized structures with each basis set and through performing single point energy calculations on Cu(II):His_3 and Asp. The binding energy of Asp was calculated as well.

Basis Set	Cu(II):His_3Asp Total Energy (Hartree)	Cu(II):His_3 Total Energy (Hartree)	Asp Total Energy (Hartree)	Binding Energy (kcal mol^{-1})
6-31G*	-3811,7815	-3296,3404	-515,1076	-209,26
6-31G**	-3811,8657	-3296,4086	-515,1234	-209,47
cc-pVDZ	-3812,2382	-3296,7658	-515,1468	-204,31
Ahlrichs-VDZ	-3809,4736	-3294,5954	-514,5541	-203,43
Ahlrichs-VTZ	-3812,0431	-3296,5843	-515,1528	-192,02
Def2-SVPD	-3810,4886	-3295,3678	-514,8192	-189,27
Def2-TZVP	-3812,9076	-3297,2553	-515,3487	-190,48
LANL2DZ-ECP	-2367,2858	-1851,9257	-515,0489	-195,26

Table 3. The total energies calculated for Cu(II):His_3Glu, Cu(II):His_3 and Glu using the optimized structures with each basis set and through performing single point energy calculations on Cu(II):His_3 and Glu. The binding energy of Glu was calculated as well.

Basis Set	Cu(II):His_3Glu Total Energy (Hartree)	Cu(II):His_3 Total Energy (Hartree)	Glu Total Energy (Hartree)	Binding Energy (kcal mol^{-1})
6-31G*	-3851,0868	-3296,3408	-554,4208	-204,08
6-31G**	-3851,1741	-3296,4082	-554,4399	-204,53
cc-pVDZ	-3851,5482	-3296,7661	-554,4644	-199,41
Ahlrichs-VDZ	-3852,2307	-3294,5966	-553,8326	-193,93
Ahlrichs-VTZ	-3851,3476	-3296,5842	-554,4694	-184,51
Def2-SVPD	-3849,7721	-3295,3690	-554,1103	-183,75
Def2-TZVP	-3852,2284	-3297,2556	-554,6771	-185,58
LANL2DZ-ECP	-2406,5832	-1851,9249	-554,3595	-187,49

Table 4. The total energies calculated for Cu(II):His_3Tyr, Cu(II):His_3 and Tyr using the optimized structures with each basis set and through performing single point energy calculations on Cu(II):His_3 and Tyr. The binding energy of Tyr was calculated as well.

Basis Set	Cu(II):His_3Tyr Total Energy (Hartree)	Cu(II):His_3 Total Energy (Hartree)	Tyr Total Energy (Hartree)	Binding Energy (kcal mol^{-1})
6-31G*	-3929,4664	-3296,3397	-632,8107	-198,28
6-31G**	-3929,5567	-3296,4081	-632,8326	-198,28
cc-pVDZ	-3929,9291	-3296,7584	-632,8617	-193,90
Ahlrichs-VDZ	-3927,0554	-3294,5935	-632,1596	-189,65
Ahlrichs-VTZ	-3929,7332	-3296,5793	-632,8595	-184,76
Def2-SVPD	-3928,1050	-3295,3656	-632,4493	-182,00
Def2-TZVP	-3930,6288	-3297,2536	-633,085	-181,79
LANL2DZ-ECP	-2484,9517	-1851,9234	-632,7333	-185,12

These findings are in accord with the calorimetric measurements conducted by Farkas and co-workers (115). Specifically, they presented more stable Cu(II):Asp and Cu(II):AspGly complexes as to the Cu(II):Glu and Cu(II):GluGly species, respectively. Moreover, Gassmann and co-workers showed that Asp is more firmly coordinated to Cu(II)-L-His than Glu (116) using electrophoresis. Same migration time tendency was also shown for Cu(II)-aspartame (117). These experimental results support our theoretical findings. Zare and co-authors showed a quicker migration time for Tyr as to Glu and Asp through capillary electrophoresis measurements (116, 117). However, this result could be caused by the utilization of di-dansyl-tyrosine in their measurements that yields a complex with different charge as to Cu(II) complexes with Asp or Glu, which decreases the migration time instead of tighter coordination. In excellent agreement with our theoretical results, the fluorescence measurement data indicate that Asp is more firmly coordinated to Cu(II)-L-His than Tyr. In addition, Rickard and co-authors conducted first principles calculations on Cu(II) species with either CH_3S^-, NH_3, 4-CH_3-imidazole, CH_3NH_2, $C_6H_5O^-$, or $CH_3CO_2^-$ to study possible coordinating amino acid moieties and the other three coordinating moeities represented by NH_3 or H_2O (68). Specifically, they presented that $CH_3CO_2^-$ binding is preferred over $C_6H_5O^-$ binding when the other ligands are nitrogen atoms and thus Asp and Glu binding is more favorable than Tyr binding, which is in excellent accord with our investigations using full-length amino acid ligands.

In this study, we have performed a detailed investigation of the structural and thermodynamic properties along with aggregation propensities of Cu(II)-bound Aβ40 and Aβ42 in aqueous solution using the new potential functions (84). Furthermore, we investigate the differential impact of different proposed coordination mechanisms of the species I coordination complex including three histidine residues. To the best of our knowledge, this is the first study to present the structural and thermodynamic differences upon Cu(II) binding via either the His_3Asp1 or His_3Tyr10 residues to the Aβ40 and Aβ42 peptides using the new potential functions. Results are compared to those obtained for Cu(II):Aβ40 and Cu(II):Aβ42 with Cu(II) binding via the His_3Glu11 residues and to those of apo Aβ (85, 88). Furthermore, results reveal that varying coordination chemistries and alloforms impact the calculated structural and thermodynamic properties.

The calculated average thermodynamic properties; enthalpy (*H*), entropy (*S*) and Gibbs free energy (*G*) for the apo and Cu(II)-bound Aβ alloforms including all three simulated binding sites are listed in Table 5. The conformational free energy values (*G*) indicate that the free Aβ40 and Aβ42 structures are more favorable than their Cu(II)-bound counterparts regardless of the chosen Cu(II) coordination chemistry. Specifically, the Cu(II)-bound Aβ40 and Aβ42 structures are less preferred than the free Aβ40 and Aβ42 structures by at least 500 kJ mol^{-1}. This result illustrates that Aβ40 and Aβ42 aggregation is increased upon Cu(II) binding since the reactivity of Cu(II):Aβ is increased due to less stability as to apo Aβ . Therefore, our results are in accord with experiments that report an increase in Cu(II)-bound Aβ peptide aggregation (2, 6, 8, 15, 17, 118, 119). We do observe that there is a difference in the thermodynamic preference of the Cu:Aβ structures that depends on the coordination chemistry. Cu(II)-bound Aβ40 peptide structures are less preferred than the

free-Aβ40 peptides by 930.1 kJ mol^{-1}, 589.0 kJ mol^{-1}, and 794.8 kJ mol^{-1} for the Cu:His_3Asp1, Cu:His_3Glu11 and Cu:His_3Tyr10 binding sites, respectively. For the Aβ42 peptides, the Cu(II)-bound peptides are less preferred than the free Aβ42 peptide by 886.8 kJ mol^{-1}, 536.2 kJ mol^{-1}, and 735 kJ mol^{-1} for the Cu:His_3Asp1, Cu:His_3Glu11 and Cu:His_3Tyr10 binding sites, respectively. This result suggests that the coordination chemistry involving the Glu11 residue results in the most preferred Cu(II)-bound Aβ conformations while the coordination chemistry involving the Asp1 residue results in the least preferred Cu(II)-bound Aβ conformations, regardless of the chosen alloform. Xu *et al.* reported binding Gibbs free energy values for different Cu(II) and Aβ16 conformations (not full-size Aβ40/Aβ42) that vary between -1288 kJ/mol and 303 kJ/mol (87). Furthermore, they reported that Cu(II)-bound Aβ16 species are by 232.7-420.9 kJ/mol less stable than the free Aβ16 peptide. However, we should note here that their force field parameters were not developed using full-length amino acid residues but model small size imidazole, acetic acid, and formamide structures. Moreover, Mantri *et al.* reported a less favorable potential energy by up to 477 kJ/mol for Cu(II)-bound Aβ42 in comparison to free Aβ42 (139). These trends are in agreement with our findings. Due to the assumption that the least thermodynamically preferred metallopeptide structures are more likely to aggregate (56, 83, 85, 88, 96, 108, 109), our results also indicate that the coordination chemistry can influence the aggregation rate as well. Therefore, the aggregation rate of the Cu(II)-Aβ alloforms depending on the coordination chemistry would be on the order of Cu:His_3Glu < Cu:His_3Tyr < Cu:His_3Asp for both Aβ alloforms. In addition to the binding site differences, we also note that the Cu(II)-bound Aβ40 structures are more preferred than Cu(II)-bound Aβ42 structures by between 56.2 and 72.7 kJ mol^{-1}, which is the same trend observed for the free Aβ40 and Aβ42 alloforms with a difference of 116.0 kJ mol^{-1} (56, 85, 88, 96). Therefore, we predict that the Cu(II)-bound Aβ42 alloforms will aggregate more readily than the Cu(II)-bound Aβ40 alloforms regardless of the Cu(II) ion coordination chemistry. The same trend is also observed for the apo-Aβ40 and Aβ42 alloforms ($\Delta G_{Aβ40\text{-}Aβ42}$ = -116.0 kJ mol^{-1}), which agrees with experimentally reported increased aggregation rates of the Aβ42 peptide in comparison to the Aβ40 peptide in aqueous solution (2, 6, 8, 15, 17, 118, 119).

Table 5. The calculated enthalpy (*H*), entropy (-*TS*), and Gibbs free energy (*G*) of the simulated Cu(II)-bound Aβ40 and Aβ42 alloforms with varying coordination chemistries in aqueous solution.

	<*H*> (kJ mol^{-1})	**-*T*<*S*> (kJ mol^{-1})**	**<*G*> (kJ mol^{-1})**
apo-Aβ40	-2788.2 (±55.6)	-2114.4 (±9.9)	-4902.5 (±45.9)
Cu:His_3Asp1-Aβ40	-1884.7 (±43.0)	-2087.7 (±9.4)	-3972.4 (±33.8)
Cu:His_3Glu11-Aβ40	-2232.4 (±11.1)	-2081.0 (±0.8)	-4313.5 (±10.7)
Cu:His_3Tyr10-Aβ40	-1998.8 (±46.1)	-2109.0 (±12.8)	-4107.7 (±33.8)
apo-Aβ42	-2579.9 (±24.2)	-2206.6 (±4.1)	-4786.5 (±20.3)
Cu:His_3Asp1-Aβ42	-1719.1 (±13.4)	-2180.6 (±7.4)	-3899.7 (±7.2)
Cu:His_3Glu11-Aβ42	-2072.7 (±19.4)	-2177.6 (±3.2)	-4250.3 (±16.6)
Cu:His_3Tyr10-Aβ42	-1854.2 (±27.6)	-2197.4 (±6.4)	-4051.5 (±21.3)

Aβ accumulation inhibition in transgenetic mice utizilizing Cu chelators was reported by Bush and co-workers (2, 23). Additionally, the same group presented a high affinity for Cu coordination with Aβ42 in the presence of trace divalent copper ion contamination (2, 23, 119). However, they also presented that Cu(II) coordination with Aβ40 has lower affinity and thus they expected less self-aggregation for Aβ40. The less favorable coordination of Cu(II) with Aβ40 and Aβ42 in comparison to our earlier studies regarding Zn(II):Aβ40 and Zn(II):Aβ42 is also noted in our investigations. We anticipate though an increased propensity toward species that play a role in oligomerization and fibrillization because of larger conformational Gibbs free energy values (see Table 5 and Ref. 85 and 96). Furthermore, the coordination of these transition metals with Aβ40 via fluorescence spectroscopy was investigated by Palumaa *et al.* (39). They found that Cu(II) and Aβ40 bind to one another and that Cu:Aβ40 is active toward other species in the solution. Thermodynamic results (Table 5) including those that we presented for Zn(II):Aβ40 and Zn(II):Aβ42 (96) as well as Cu(II):Aβ with a Cu:His_3Glu coordination site (85) present that Cu(II):Aβ40 is expected to be active toward ligands because of its larger Gibbs free energy and associated reduced conformational stability in comparison to Zn(II):Aβ40. Additionally, Atwood and co-workers showed that Cu:Aβ is reactive toward other ligands and reported dityrosine croos-linking for Cu:Aβ (28, 120, 121). NMR measurements by

Zagorski and co-workers showed that Cu(II) coordination with Aβ yields nonfibrillar amorphous conformations and fast aggregation (9). Even though Cu(II):Aβ interacted with other compounds and disturbed high-quality K_D measurements of Cu(II) with Aβ, Faller reported the dissociation constants for Cu(II) and Zn(II) in an aqueous solution medium at neural pH as 10 to 200 pM and 1 to 20 μM, respectively (122). The binding of Cu(II) to NTA (chelator) influenced the accuracy of these measurements because Cu:NTA has a similar K_D value to Cu:Aβ (122). Smaller dissociation constants for Cu(II):Aβ in comparison to Zn(II):Aβ may be due to the different thermodynamic stabilities that we report here and in our previous studies. Experiments presented also similar binding affinities for Zn:Aβ40 and Zn:Aβ42 and our conformational Gibbs free energies that we reported recently for Zn:Aβ40 and Zn:Aβ42 are similar (124, 125).

Experiments presented that the aggregation building blocks are monomeric Cu(II):Aβ and Zn(II):Aβ in 1:1 ratio utilizing NMR spectroscopy and chromatography measurements (121-124). Cu(II) and Aβ40 were shown to form stable but soluble 1:1 species, however, K_D meauserements were influenced by buffer complexes that bound to Cu(II) as ligands (39). An active Cu(II):Aβ complex toward buffer species is expected because of our greater Gibbs free energy values for Cu(II):Aβ40 and Cu(II):Aβ42 that are presented in Table 5 in comparison to our values that we recently showed for Zn(II):Aβ40 and Zn(II):Aβ42 (96). Extensive studies were performed for gaining insights into the reversible formation of Cu(II) and Zn(II) complexes with Aβ (see Ref. 39). The binding affinity values fluctuate enormously, for instance, values varying between 10 nmol/L to 300 μmol/L were reported for Zn(II):Aβ (96). Values fluctuating between 0.1 nmol/L – 10 μmol/L were reported for Cu:Aβ (124-127). Thermodynamic studies provide insights onto these debates since experiments yield uncertantities in the vicinity of buffers. Moreover, our investigations support those of Hane *et al.* They presented greater dimerization tendencies for Aβ upon Cu(II) coordination (15). These findings present a less stable but more reactive monomeric Cu:Aβ toward Aβ. Amorphous structures were reported for Zn:Aβ while more ring-like and extended conformations were shown for Cu:Aβ, which in turn results in Cu:Aβ adopting varying oligomerization and fibrillization processes (see below tertiary structural properties subsection) (125-127).

In addition to the conformational Gibbs free energies, we evaluated the conformational favorabilities of the free and Cu(II)-bound Aβ40 and Aβ42 peptides via potential of mean force (PMF) calculations along in conjunction with end-to-end distance (R_{E-E}) and radius of gyration (R_g) (Figures 2A and 2B). In our previous works, we have shown that this method reveals differences in the conformational ensembles resulting from alloform length, mutation and zinc coordination (56, 85, 88, 96, 108, 109). Figure 2A displays the PMF surfaces for the free Aβ40 and Cu(II):Aβ40 peptides including different Cu(II) binding sites. Favorable PMF basins located at R_g values from 10.75 Å to 11.75 Å for basin IA and from 9.1 Å to 13.2 Å for basin IB and at R_{E-E} values varying from 10 Å to 17 Å for basin IA and from 17.6 Å to 34.8 Å for basin IB are detected. Paramounting energy barriers larger than 1 k_BT is required for structural transformation between basins IA and IB. Upon Cu(II) coordination via the His_3Asp1 binding site, the basin IA R_{E-E} values shift to 2.5 Å to 5 Å (Cu(II):His_3Asp1-Aβ40, basin IA) and basin IB shifts to R_g values between 9.5 Å to 10.5 Å along with R_{E-E} values 7.5 Å to 17.5 Å. The energy barrier for transitions between these two preferred basins is increased to greater than 2 k_BT. On the other hand, for the Cu(II)-bound structures utilizing the His_3Glu11 binding site, only one preferred basin is present at R_g values of 9.5 Å – 11 Å along with R_{E-E} values of 7.5 Å – 35 Å. Transitions between the structures located in this basin do not desire overriding large energy barriers. For the Cu:His_3Tyr10-Aβ40 peptide, basin IA is similarly located in comparison to the apo-Aβ40 peptide with R_g values of 10.25 Å – 11.3 Å and R_{E-E} values of 10.5 Å – 16.5 Å. However, the basin IB structures have a smaller range of R_g values (9.75 Å – 10.75 Å) and R_{E-E} values in comparison to the apo-Aβ40 structures even though transition between the two basins still require overriding energy barriers with a height of greater than 1 k_BT.

The PMF surfaces along R_g and R_{E-E} for the wild-type and free and Cu(II):Aβ42 peptides are presented in Figure 2B. Aβ42 shows two preferred basins located at R_g values of 10.5 Å – 11.6 Å and 10.1 Å – 10.9 Å and R_{E-E} values of 10 Å – 17 Å and 24 Å – 32 Å. Overriding of these two preferred basins via transitions needs energies of greater than 1 k_BT. Upon Cu(II) binding via the His_3Asp1 amino acid residues, the basin IA R_{E-E} values shift to between 2.5 Å to 5 Å, which is similar to the affect of Cu(II) binding via the His_3Asp1 coordination chemistry to the Aβ40 peptide. However, basin IB R_g and R_{E-E} values are expanded to 9.6 Å – 11.4 Å and 6 Å – 25.5 Å, respectively. This increase of R_g and R_{E-E} in the basin IB structures is the vice versa trend of that observed for Cu(II) binding via the same

coordination chemistry of the Aβ40 alloform. In addition, basin transitions require paramounting energy barriers of greater than 1 k_BT and not greater than 2 k_BT as observed for the Aβ40 alloform. Interestingly, the Cu:His_3Asp1-Aβ42 peptide also exhibits a third preferred PMF basin (basin IC) at R_g values of 13.7 Å – 14.2 Å and R_{E-E} values of 15.5 Å – 17.5 Å. Transitions between the basin IC structures and the basin IA or basin IB structures involve overriding energy barriers of greater than 2 k_BT. For the Aβ42 structures that bind Cu(II) via the His_3Glu11 binding site, two preferred basins are detected. These have R_g values of 9.8 Å – 11 Å for basin IA structures and 10.1 Å – 10.8 Å for basin IB structures along with R_{E-E} values of 5.5 Å – 16 Å and 20 Å – 27.5 Å, respectively. Larger than 1 k_BT barriers exist between these preferred basins. This effect of the Cu(II):Aβ42 with the Cu:His_3Glu11 binding site shows different trends than for Cu(II):Aβ40, which possesses a single preferred basin (see above). Regarding the Cu:His_3Tyr10-Aβ42 peptide, we observe a single most preferred PMF basin at R_g values of 10.1 Å – 11.5 Å along with R_{E-E} values of 9.5 Å – 22.5 Å, which is a different conformational ensemble than the two favorable PMF basins presented for the Cu(II):His_3Tyr10-Aβ42 peptide. Overall, these data present that the Cu(II) binding to the Aβ40 and Aβ42 alloforms impacts the conformational ensemble of these two peptides and that the effect on the conformational ensemble depends on the chosen coordination site. Furthermore, the impact of Cu(II) coordination - depending on the coordination chemistry of the Cu(II) ion - varies between the two different Aβ alloforms.

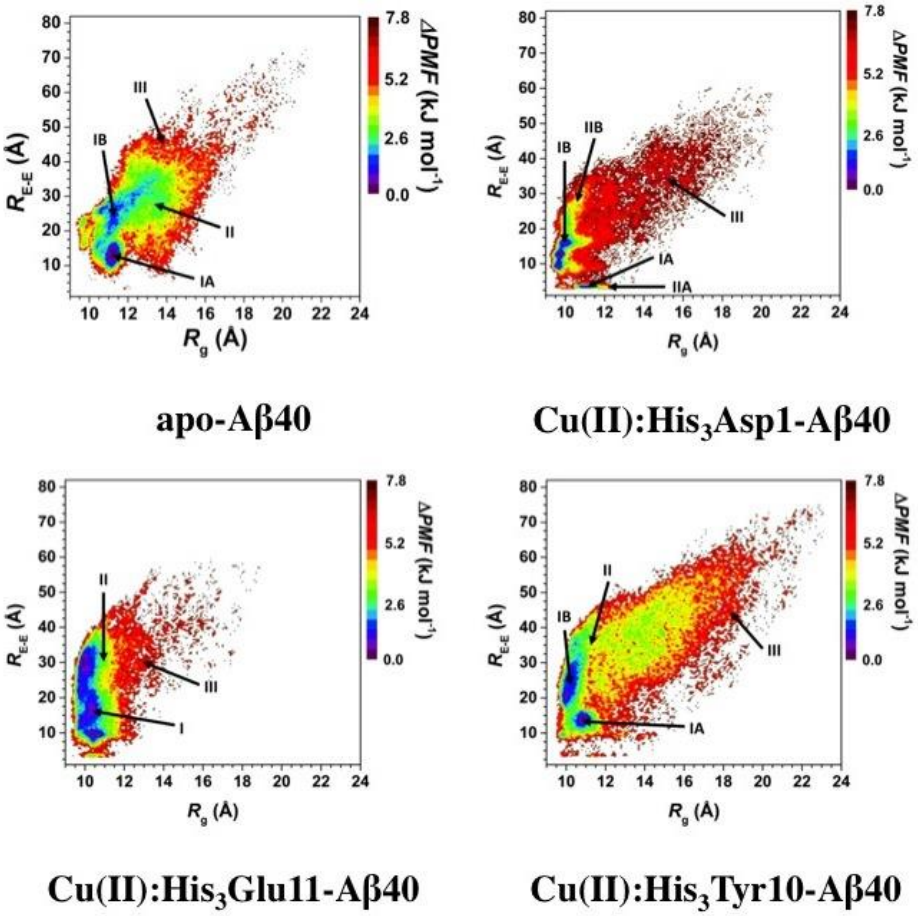

Figure 2A. Potential of Mean Force Surfaces of the apo and Cu(II)-bound Aβ40 Peptides. Potential of mean force (ΔPMF) of the Aβ40, Cu(II):His_3Asp1-Aβ40, Cu(II):His_3Glu11-Aβ40, and Cu(II):His_3Tyr10-Aβ40 structures along the coordinates of the radius of gyration (Rg) and end-to-end distance (R_{E-E}).

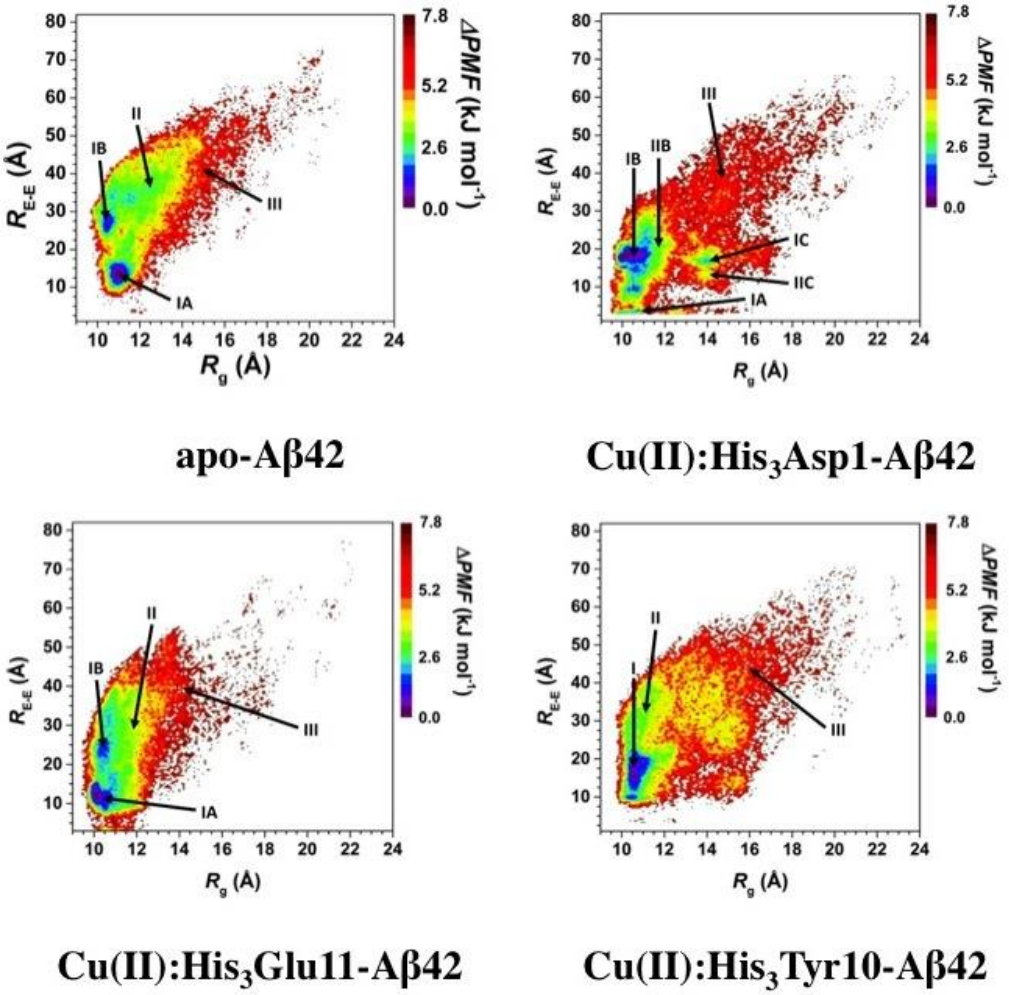

Figure 2B. Potential of Mean Force Surfaces of the apo and Cu(II)-bound Aβ42 Peptides. Potential of mean force (ΔPMF) of the Aβ42, Cu(II):His_3Asp1-Aβ42, Cu(II):His_3Glu11-Aβ42, and Cu(II):His_3Tyr10-Aβ42 structures along the coordinates of the radius of gyration (*R*g) and end-to-end distance (R_{E-E}).

Our R_g values for aqueous Cu(II):Aβ40 and Cu(II):Aβ42 with varying coordination chemistries are illustrated in Figure S7 (supporting information section). Upon Cu(II) coordination, Aβ40 and Aβ42 become more compact. In comparison to our recent studies, Zn(II):Aβ40 is more compact than Cu(II):Aβ40 (85). The same trend is also obtained for Cu(II):Aβ42 and Zn(II):Aβ42 (85). Less compact and less stable disordered metalloprotein conformations are more active toward other species in the solution. Therefore, we expect Cu(II):Aβ to be more active than Zn(II):Aβ, which is in accord with experimental observations (see above). Calculated R_g values support our thermodynamic findings, which were presented and discussed above. IMS-MS experiments were conducted by Sietkiewicz *et al*. They measured the compactness changes of Aβ upon Zn(II) and Cu(II) coordination (126). In agreement with earlier investigations, they noted that the Asp23-Lys28 salt bridge stabilizes the conformations and provides compactness into the structures while Gly25 is active in extended oligomeric structure formations. Based on their results, the compact forms of Aβ dominate upon Zn(II) or Cu(II) addition. This finding is in accord with our data. With the inclusion of our previous studies, we find that transition metal ion coordination increase the compactness of monomeric Aβ in an aqueous solution medium. Moreover, the Asp23-Lys28 salt bridge is reduced in its abundance upon Cu(II) binding and disappears upon Zn(II) coordination with Aβ (details are provided below). A similar trend is observed in Aβ40 structures for the Glu22 and Lys28 salt bridge upon Zn(II) and Cu(II) ion coordination. In addition, intramolecular interations between the N- or C-terminal and CHC regions are reduced in probability upon Cu(II) binding (results are illustrated below). Our R_g values agree with light scaterring experiments and previous theoretical studies (127-133).

Secondary structure abundances of the apo and Cu(II)-bound Aβ40 peptides with different coordination chemistries are presented in Figure 3. Within the N-terminal region (Asp1-Lys16), a serious decrease (between 5% to 40%) in the abundance of the helical (α- and 3_{10}-helix), β-sheet and turn secondary structural elements occurs upon transition metal ion coordination to the Aβ40 peptide independent of the coordination chemistry. This decrease of ordered secondary structure component formation is expected due to this region participating in the Cu(II) coordination for all binding sites. An exception is the 15% - 52% increase in 3_{10}-helical content for residues Val12-Gln15 in the Cu:His_3Glu11-Aβ40 structures in comparison to the apo-Aβ40 structures. Furthermore, only residues Ala2, His13 and His14 in the N-terminal region present a larger turn content of greater than 10% for the Cu:His_3Asp1-Aβ40 peptide. We also note that the α-helix and β-sheet content is decreased by between 5% and 35% in the central hydrophobic core (Leu17-Ala21; CHC) region upon Cu(II) binding independent of the coordination chemistry except for the β-sheet composition at Leu17 and Val18 upon Cu(II) binding via the His_3Asp1 binding site. However, the 3_{10}-helical prominence at Leu17-Phe19 is more significant (by ≥ 5%) upon copper ion binding either to the His_3Asp1 or His_3Glu11 coordination sites. Additionally, the turn content at residues Phe19 and Phe20 in the Cu:His_3Asp1-Aβ40 peptide, Val18-Ala21 in the Cu:His_3Glu11-Aβ40 peptide, and Val18 in the Cu:His_3Tyr10-Aβ40 increases by at least 10% in comparison to apo Aβ40 in aqueous solution. The mid-domain (Glu22-Ala30) and C-terminal (Ile31-Val40) also presents a few residues with significant differences in the formed secondary structure content upon Cu(II) coordination. Specifically, the α-helix abundance at Glu22 and Asp23, the β-sheet content at Ser26-Ile32 and the turn content at Val24-Ser26 decrease by ≤ 25% upon copper ion coordination to Aβ40 independent of the coordination chemistry variations. Contrastingly, the 3_{10}-helix content at residues Ile32-Val36 is more significant (by ≥ 10%) upon Cu(II) binding to Aβ40 for all coordination sites. However, we also note a differential impact on secondary structure formations of the Aβ40 peptide upon Cu(II) binding depending on the coordination chemistry. Specifically, the α-helix and the 3_{10}-helix abundance at Val24-Lys28 and the β-sheet probability at Val39 increase in the Cu:His_3Glu11-Aβ40 peptide as to apo Aβ40. Furthermore, β-sheet at Leu34 in Cu:His_3Asp-Aβ40 and at Val36 and Val39 in the Cu:His_3Tyr10-Aβ40 peptide is higher by at least 5% than in the apo-Aβ40 peptide.

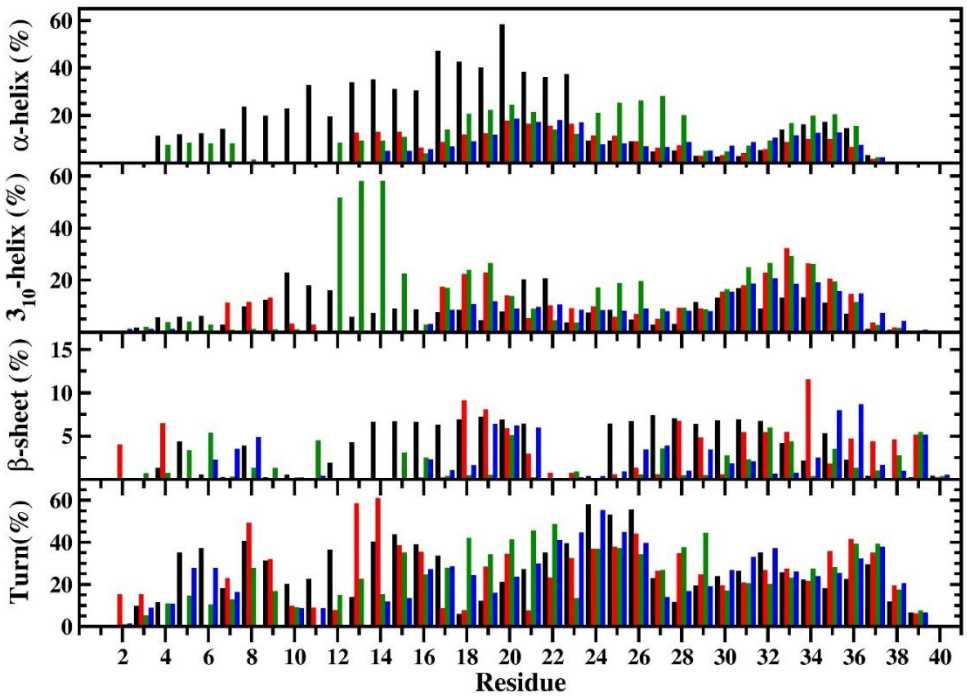

Figure 3: Residual Secondary Structure Abundances of the apo and Cu(II)-bound Aβ40 Peptides. Secondary structure abundances per residue of the Aβ40 (black), Cu(II):His_3Asp1-Aβ40 (red), Cu(II):His_3Glu11-Aβ40 (blue), and Cu(II):His_3Tyr10-Aβ40 (green) structures in an aqueous solution. The π-helix and coil structures are not displayed.

Figure 4 presents the secondary structure probabiities of apo- and copper ion-bound Aβ42. α- and 3_{10}-helix as well as turn content of the N-terminal region of the Aβ42 peptide decreases significantly upon Cu(II) binding regardless of the binding site except for residue His13 in the Cu:His_3Asp1-Aβ42 peptide and residues Val12-Gln15 in the Cu:His_3Glu11-Aβ42 peptide, which display vice versa trends. Interestingly, the increase in 3_{10}-helical content with the Cu:His_3Glu11 binding site was also detected for Aβ40. Unlike what we observed with the Aβ40 peptide, residues Tyr10-Val12 of Cu:His_3Asp1-Aβ42, Phe4-Asp7 of Cu:His_3Glu11-Aβ42, and Val12 of Cu:His_3Tyr10-Aβ42 present a larger abundant (> 5%) β-sheet content as to the apo-Aβ42 peptide. The 3_{10}-helical content in the CHC region of Aβ42 is not significantly impacted by Cu(II) binding to the His_3Asp1 but we do note a signifance reduction in α-helical abundance for residues Leu17-Phe19. Instead, a considerable reduction in β-sheet probability for residues Leu17-Phe19 is displayed in the Cu:His_3Asp1-Aβ42 structures as to the apo-Aβ42 peptide while the opposite trend is presented for residues Phe20 and Ala21. When Cu(II) is bound to the His_3Glu11 residues, we observe a boost in α-helical probability for Phe19-Ala21 and in 3_{10}-helix content for Leu17-Ala21 as to the apo-Aβ42 peptide. However, residues Leu17 and Val18 present α-helix abundance reduction (> 10%) upon Cu(II) coordination to the three His residues and the Glu11 residue. Furthermore, Leu17 and Phe19 adopt a larger β-sheet probability (≥ 5%) in the structures of Cu:His_3Glu11-Aβ42 as to apo-Aβ42 while the opposite trend was detected for Phe20 and Ala21. Cu:His_3Tyr10-Aβ42 peptide´s CHC region also presents significant differences from the apo-Aβ42 peptide. Namely, the α-helix abundance of residues Leu17 and Val18 as well as the β-sheet abundance of Phe20 and Ala21 decreases by at least 10% and 5% respectively when Cu(II) binds to the His_3Tyr10 residues. On the other side, we observe a significant increase in 3_{10}-helix content for residues Val18-Ala21 and in β-sheet probability of residues Leu17-Phe19 for the Cu:His_3Tyr10-Aβ42 structures as to the apo-Aβ42 peptide. We note that residues Glu22-Val42 and Gly25-Asn27 present significant decreases in turn and β-sheet contents for all three Cu(II)-bound Aβ42 peptides as to apo-Aβ42. Furthermore, we also note a boost in α-helical probability of residues Glu22 and Asp23 of the Cu:His_3Asp1-Aβ42 structures and residues Glu22-Lys28 of the Cu:His_3Glu11-Aβ42 structures as to apo-Aβ42. However, we do observe helical probability reduction of Gly29-Met35 for all three Cu(II)-bound Aβ42 peptides in comparison to the apo-Aβ42. The C-terminal β-sheet content increases upon Cu(II) binding for all three coordination sites except at residues Ile31-Leu24 and Ala42 of the Cu:His3Asp1-Aβ42 peptide, Val36 and Gly38 of the Cu:His3Glu11-Aβ42 peptide, and Gly38 and Ala42 of the Cu-His3Tyr10-Aβ42 peptide.

In addition to the differences observed for each alloform upon Cu(II) binding, we also observe specific differences between the Cu(II)-bound Aβ40 and Aβ42 alloforms for each binding site (Figures 3 and 4). In the case of the Cu:His_3Asp1-Aβ alloforms, we note an increase in α-helical content of at least 10% for residues His13-Gln15 and Gly29-Val36. However, 3_{10}-helical content is significantly decreased (> 10%) for residues Asp7-Gly9 and Leu17-Phe19. Additionally, the β-sheet content of residues Tyr10-Val12, Lys16-Ala21, and Met35-Ala41 is increased in the Aβ42 rather than Aβ40 alloform when Cu(II) is bound to the His_3Asp1 residues. However, an opposite trend is observed at Lys28, Gly29, and Ile31-Leu34. Furthermore, the turn content of residues His13-Lys16, Phe19, Phe20, Asn27, Lys28 and Met35-Gly37 is decreased in the Aβ42 alloform in comparison to the Aβ40 alloform for the Cu:His_3Asp1 binding site.

For the Cu:His_3Glu11-Aβ alloforms, α-helical probability increase in the Aβ42 alloform as to the Aβ40 alloform is observed for residues Glu22 and Asp23. Ser26-Lys28 display an opposite trend. The 3_{10}-helical probability at Val24-Ser26 and Gly33-Met35 reduces from the Cu:His_3Glu11-Aβ40 to the Cu:His_3Glu11-Aβ42 alloform. The β-sheet abundances present that the β-sheet content of the Cu:His_3Glu11-Aβ42 peptide is boosted at residues Phe4-Asp7, Lys16-Ala21, Leu34-Gly37, Ile41 and Ala42 as to the Cu:His_3Glu11-Aβ40 peptide. Residues Leu17-Glu22 display a reduced turn probability in the Cu:His_3Glu11-Aβ42 structures rather than the Cu:His_3Glu11-Aβ40 peptide while a vice versa trend is observed for the both Ile residues (Ile31/Ile32).

Corresponding analysis of the Cu:His_3Tyr10-Aβ40 and Cu:His_3Tyr10-Aβ42 peptides reveals alloform differences between these two Cu(II)-bound peptides as well. Namely, the α-helical abundance of residues Glu22-Gly25 is increased in the Cu:His3Tyr10-Aβ(1-42) alloform as to Cu:His3Tyr10-Aβ(1-40). Furthermore, 3_{10}-helix probability is increased for residues Leu17-Ala21 and Gly38-Ile41 in the Aβ42 alloform rather than Aβ40 alloform upon Cu(II) coordination to His3Tyr10. Contrastingly, the opposite trend is observed for the overall helical content of residues Lys28-Ile32. Additionally, the abundance of

turn structure for residues Lys16-Val24 and Ala30-Met35 is increased in the Cu:His_3Tyr10-Aβ40 rather than the Cu:His_3Tyr10-Aβ42 alloform. Despite, the turn content of residues Asn27-Gly29 display the vice-versa trend. Similar to the other two Cu(II) binding sites, the β-sheet content in the Cu:His_3Tyr10-Aβ42 alloform is significantly increased in comparison to the Cu:His_3Tyr-Aβ40 alloform. Specifically, residues Val12, Leu17-Glu22, Gly29, Ile31-Met35 and Val39-Ile41 have a significant (> 5%) abundance of β-sheet component in Cu:His_3Tyr10-Aβ42 rather than the Cu:His_3Tyr10-Aβ40 alloform.

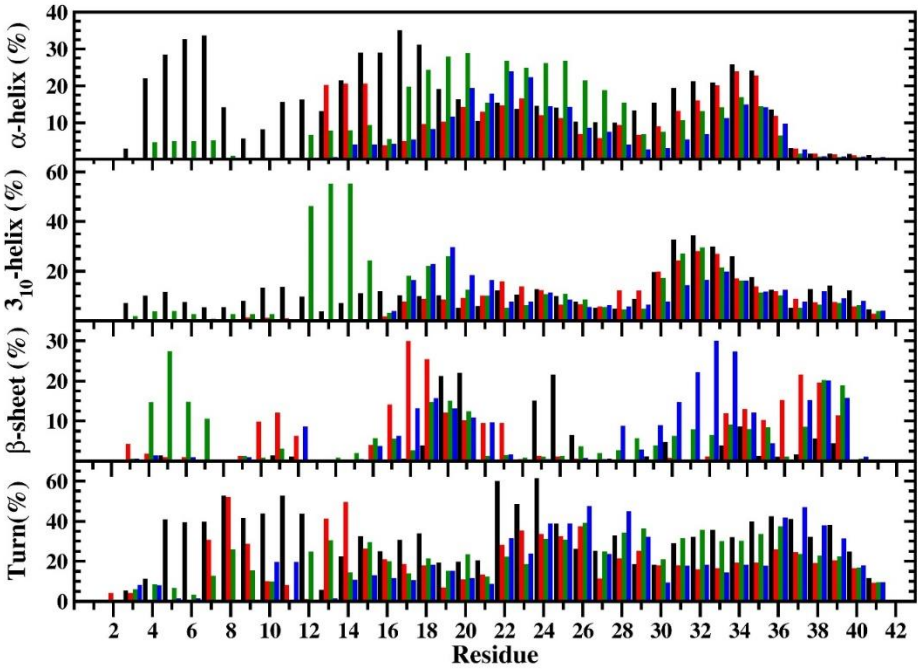

Figure 4: Residual Secondary Structure Abundances of the apo and Cu(II)-bound Aβ42 Peptides. Secondary structure abundances per residue of the Aβ42 (black), Cu(II):His_3Asp1-Aβ42 (red), Cu(II):His_3Glu11-Aβ42 (blue), and Cu(II):His_3Tyr10-Aβ42 (green) structures in an aqueous solution. The π-helix and coil structures are not displayed.

β-sheet structure formations, especially in the CHC and C-terminal regions, is a central event in aggregation processes of the Aβ peptides (56, 83, 85-87, 96, 108, 109 and references therein). The results presented predict β-sheet formation variations in the Aβ alloforms upon Cu(II) binding with varying coordination chemistries using our new potential functions. From these results, we note a similar or reduced β-sheet formation in the CHC region of Aβ40, depending on the Cu(II) ion coordination chemistry. However,the C-terminal region at Val36-Ile31 represents an increased or similar β-sheet probability upon Cu(II)-binding. Aβ42 presents β-sheet probability boost in the CHC region (Leu17-Phe19) and the C-terminal region (Ala30-Ile41) upon Cu(II) binding for all three binding sites. Results illustrate that divalent copper ion binding enhances Aβ42 aggregation moreso than Aβ40 aggregation. Furthermore, Cu(II)-bound Aβ42 β-sheet probability is significantly higher than the Cu(II)-bound Aβ40 alloforms regardless of the coordination chemistry in both regions (CHC/C-terminal regions). Therefore, reported enhaned β-sheet content of the C-terminal region of the apo-Aβ42 as to the apo-Aβ40 peptide is not affected and is even enhanced for some residues. This finding indicates that the previously reported boosted aggregation rate of apo-Aβ42 as to the apo-Aβ40 peptide is not affected and may even be enhanced by Cu(II) coordination.

Boopathi and Kolandaivel investigated the secondary structures of Zn(II):Aβ40 and Cu(II):Aβ40 using MD simulations for only 50 ns without special sampling methods to gain insights into the secondary structure properties of these disordered metalloproteins without mentioning thermodynamic properties and without considering coordination chemistry variations (132). The results presented herein partially agree with their findings. For instance, we also detect turn component formation with high probability at Ala21-Ala30 of Aβ40 that is associated with Asp23-Lys28 less stable salt bridge occurance in comparison to the stability of Glu22-Lys28 (Table 6). Unlike the studies by Boopathi and Kolandaivel, our findings present β-sheet occurrence with high probability in the C-terminal region of Aβ40. Furthermore, the

same group presented prominent turn structure formation in the Asp23 to Asp27 region in Cu(II):Aβ40 conformations without investigating different coordination chemistry effects (132). Using the same coordination chemistry, turn structure abundance is decreased at Gly25 and Ser26 upon copper ion coordination with Aβ40. Furthermore, several research groups illustrated the structural properties of Cu(II):Aβ without investigating the coordination chemistry influences and they utilized either a potential function possessing a nonbonded model or they used the Zn(II) force field parameters for studying Cu(II):Aβ. As mentioned before (see above), the number of electrons and coordination chemistries differ for these metalloproteins and Jahn-Teller effects should not be disregarded. Therefore, simulation results for Cu(II):Aβ using the force field parameters for the zinc ion instead of those for the copper ion might be misleading. Dong and co-workers successfully investigated the intermolecular interactions between Aβ40 and Cu(II):Aβ40 with three modified clioquinol drugs (133). They performed extensive classical molecular dynamics simulations without special sampling methods. They could not detect β-sheet occurence in Aβ or in Cu(II):Aβ. Despite, Dong and co-workers expressed the self-assembly domains (CHC and C-terminal regions), highlighting β-sheet occurence in the CHC and C-terminal regions. Furthermore, our findings for apo Aβ42 are in accord with results presented by Velez-Vega and Escobedo but they used the OPLS-AA force field parameters for the disordered peptide (134). Specifically, their results present less probable α-helix occurence in Aβ42. Additionally, MD simulations without increasing the conformational sampling with specific methods utilizing the GROMOS9643A1 force field parameters showed that some residues of Aβ42 adopt helical structures (135). Our results are in partial accord with these data. Our findings also further are in accord with this study since the C-terminal region of Aβ42 forms β-sheet component. Various clustering algorithms were utilized by Garcia *et al.* They found that some residues in the N- and C-terminal regions form β-sheet element while Ser8-Val12 adopts α-helix structure (136). Our results show support to these findings (see above). Our results for apo Aβ42 are in accord with the REMD studies by Yang and Teplow (135). The structuring of the C-terminal region of apo Aβ42 including β-sheet structure adaptation with high probability have been investigated by few additional research groups (130-137). These results agree with our findings. However, these groups did not investigate the effect of coordination chemistry differences of Cu(II) on the monomeric conformations of Aβ alloforms (Aβ40/Aβ42).

The intra-molecular interactions of the apo- and Cu(II)-coordinated Aβ40 peptides with different coordination sites are displayed in Figure 5. For the apo-Aβ40 peptide, we note abundant intra-molecular interactions within the N- and C-terminal regions, CHC and mid-domain regions as well as between the N-terminal and CHC, mid-domain and C-terminal regions. Specifically, Phe4-Arg5 interact with Leu17-Phe19, Arg5 interacts with Asp23, Val12-His13 interacts with Gly33, Leu34, Val36 and Gly37, and Gln15-Lys16 interact with Ile31, Gly33, and Met35-Val40 with abundances up to 40%. CHC and mid-domain regions interact with the C-terminal region as well; Val18-Phe19 with Val39-Val40 and Phe19-Gly25 with Gly29-Gly33 (up to 60%). Furthermore, the C-terminal region interacts with itself with abundances up to 50% between residues Ala30-Met35 and Val39-Val40.

We note – upon copper ion coordination - that these abundant intra-molecular interactions in the apo-Aβ40 peptide are significantly decreased or completely disappear depending on the coordination chemistry differences; abundant intra-molecular interactions in the C-terminal region with the C-terminus between Ala30-Met35 with Val39-Val40 are not present in any of the three Cu(II)-bound Aβ40 peptides. The interactions of the N-terminal residues Val12-His13 and Gln15-Lys16 with the C-terminal residues Ile31, Gly33, Leu34, and Met35-Val40 are significantly decreased for the Cu:His_3Asp1-Aβ40 and Cu:His_3Glu11-Aβ40 peptides and completely disappear for the Cu:His_3Tyr10-Aβ40 peptides. However, we do note the appearance of interactions between Arg5-His6 in the N-terminal with residues Val36-Val40 in the C-terminal region in the Cu:His_3Asp1-Aβ40 and Cu:His_3Glu11-Aβ40 peptides. Additionally, interactions of the CHC region with N-terminal region are shifted from residues Phe4-Arg5 to residues His13-His14 for the Cu:His_3Glu11-Aβ40 peptides and residues Asp1 and His13-His14 for the Cu:His_3Asp1-Aβ40 peptide but remain for the Cu:His_3Tyr10-Aβ40 peptide. CHC region and the C-terminal interactions through Val39 and Val40 disappear upon Cu(II) binding for all three binding sites yet interactions including residues Ala29-Met35 remain. Furthermore, mid-domain (Asp23-Ser26) and C-terminal (Ile31-Leu34) regions interactions increase when Cu(II) binds to the His_3Glu binding site in Aβ40. Finally, we observe that N-terminal and mid-domain region interactions are increased for Cu:His_3Asp1-Aβ40 and Cu:His_3Glu11-Aβ40 as to apo-Aβ40. Cu:His_3Asp1-Aβ40 peptide

presents interactions of residues Asp1, Ala2, and Phe4-Arg5 with residues Asp23, Val24, Ser26, Asn27 and Gly29 whereas the Cu:His_3Glu11-Aβ40 peptide presents interactions of residues Glu3 and Arg5-His6 with Asp23-Gly25 and Lys28-Gly33.

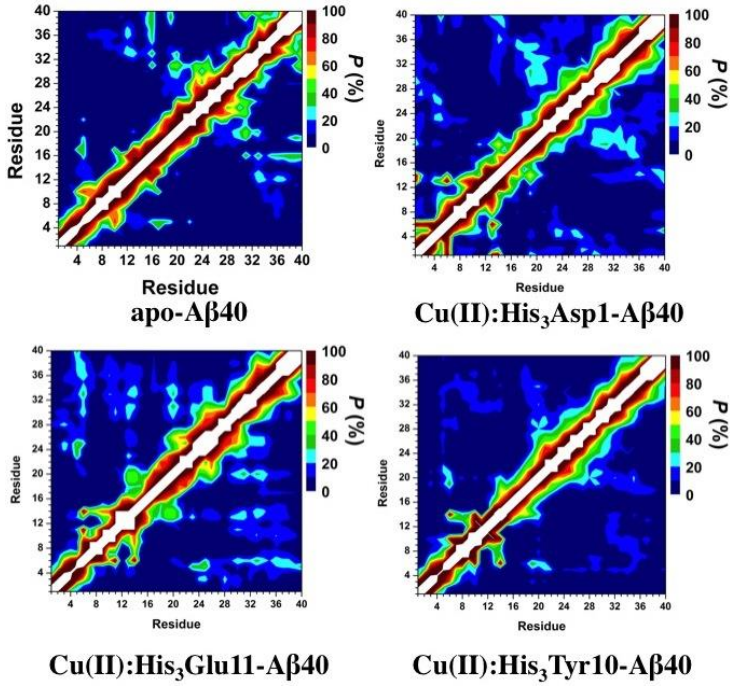

Figure 5: Intra-molecular Interaction of the apo and Cu(II)-bound Aβ40 Peptides. Calculated intra-molecular interactions for the structures of the Aβ40, Cu(II):His_3Asp1-Aβ40, Cu(II):His_3Glu11-Aβ40, and Cu(II):His_3Tyr10-Aβ40 peptides in an aqueous solution. The color scale corresponds to the computed probability (*P*) for these interactions.

Intra-molecular interactions of apo- and Cu(II)-coordinated Aβ42 with varying coordination chemistries - using our force field parameters - in aqueous solution medium are presented in Figure 6. For the N-terminal region, we note that residues Phe4-Arg5 interact with Glu11-His13. For the C-terminal region, Ile32-Leu34 interact with Val39-Val40. Interactions occur between the N-terminal and CHC regions; Phe4-Arg5 with Leu17-Phe19 and residues Gly9-Tyr10 with Leu17-Phe19. Interactions between the N-terminal and mid-domain regions exists through Phe4-His6 with Asp23-Gly29 and Gly9 with Asp23, Gly29 and Ala30. Moreover, Arg5 interacts with Ala42 and Val12 interacts with Gly33 demonstrating N-terminal and C-terminal interactions. We further note that the CHC region interacts with the mid-domain and C-terminal regions through Leu17-Ala21 with Lys28-Gly33 and Val36-Gly38.

Varying Cu(II) coordination chemistries impact significantly these interactions of apo-Aβ42. For example, N-terminal and mid-domain region interactions are less probable upon Cu(II)-coordination with only the Cu:His_3Glu11-Aβ42 and Cu:His_3Tyr10-Aβ42 peptides illustrating reduced interactions between these regions (Arg5 with Glu22). Moreover, N-terminal and CHC region interactions that we observed in apo-Aβ42 are less probable upon copper ion coordination for all three coordination sites. Abundant intra-molecular interactions occur between the residues Glu11-Gln15 (N-terminal) and the residues Val18-Ala21 (CHC regşon) of Cu:His_3Glu11-Aβ42. Residues Glu3-His6, Tyr10 and Val12 interact with Ile31, Gly33, Leu34 and Gly37-Ala42 in Cu:His_3Glu11-Aβ42 (demonstrating N- and C-terminal interactions) and for residues Asp1-Ala2 with Gly29 and Ile32-Gly33, Phe4 with Ile32, Gly9 with Val39, Glu11 with Met35-Gly38 and Arg5 with Ala42 for Cu:His_3Asp1-Aβ42. Cu:His_3Tyr10-Aβ42 exhibits N- and C-terminal interactions through residues Arg5 and Ala42. Cu:His_3Glu11-Aβ42 and Cu:His_3Tyr10-Aβ42 display CHC and C-terminal regions interactions for residues Val18-Ala21 and Ala30-Leu34. Finally, only the Cu:His_3Tyr10-Aβ42 retains an interaction between the CHC and mid-domain regions between Phe19 and Asn27.

In addition to varying Cu(II) coordination affects on the Aβ40 and Aβ42 alloforms, we also note significant alloform specific differences between the Cu(II)-bound Aβ40 and Aβ42 peptides. Cu:His_3Asp1-Aβ40 and Cu:His_3Glu11-Aβ40 show CHC and C-terminal regions as well as N-terminal and mid-domain region interactions that are not present in Cu:His_3Asp1-Aβ42 and Cu:His_3Glu11-Aβ42.

Furthermore, the number of residues interacting between the N-terminal and CHC regions is increased for Cu:His_3Asp1-Aβ42 rather than Cu:His_3Asp1-Aβ40 even though the abundance displays the vice versa trend. We also note that Cu:His_3Glu11-Aβ42 N-terminal region interacts with a higher probability with the CHC region than in Cu:His_3Glu11-Aβ40. In the case of the Cu:His_3Tyr10 binding site, we notice that intra-molecular interactions of the CHC region are more abundant with the C-terminal region for the Aβ42 alloforms but with the N-terminal region for the Aβ40 alloforms. An increase in the N-terminal interactions with the C-terminus is also observed for the Cu:His_3Tyr10-Aβ42 alloform rather than the Cu:His_3Tyr10-Aβ40 alloform. Results by Boopathi and Kolandaivel show strong N- or C-terminal and CHC regions interactions in Cu(II):Aβ42. They did not study the impact of coordination chemistry on these interactions. We detect similar interactions in Cu(II):His_3Glu-Aβ42. However, based on our findings, these interactions are more pronounced in apo Aβ42.

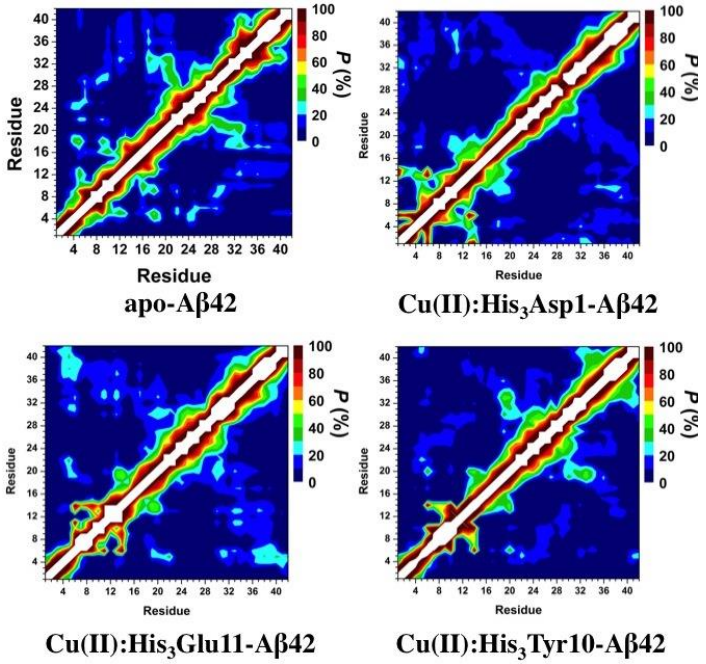

Figure 6. Intra-molecular Interaction of the apo and Cu(II)-bound Aβ42 Peptides. Calculated intra-molecular interactions for the structures of the Aβ42, Cu(II):His3Asp1-Aβ42, Cu(II):His3Glu11-Aβ42, and Cu(II):His3Tyr10-Aβ42 peptides in an aqueous solution. The color scale corresponds to the computed probability (P) for these interactions.

The formed salt bridges of apo- and Cu(II)-coordinated Aβ40 also reveal variations in the tertiary structure formations of Aβ40 upon Cu(II) binding with different coordination chemistries (Table 6). These probabilities of salt bridge formation reveal that the salt bridges between Lys16 and the C-terminus and between Arg5 and Glu22 are both significantly decreased upon Cu(II) binding for all three coordination sites. Furthermore, the salt bridge formation between Arg5 and Asp1 is significantly decreased for both the Cu:His_3Glu11-Aβ40 and Cu:His_3Tyr10-Aβ40 peptides in comparison to the apo-Aβ40. We also observe further coordination site dependent differences in the salt bridge formations. For example, the salt bridge between Arg5 and Glu3 is significantly decreased in only the Cu:His_3Asp1-Aβ40 peptide. The Cu:His_3Tyr10-Aβ40 peptide displays more abundant salt bridge formations between Arg5 and Glu11 as well as between Asp23 and Lys28 that is not observed in the other two Cu(II)-bound Aβ40 peptides. The Cu:His_3Asp1-Aβ40 and Cu:His_3Glu11-Aβ40 peptides present more abundant salt bridge formations between Arg5 and the C-terminus as well as Asp23. Lastly, the salt bridge between the N-terminus and the Glu22 residues is more abundant in the Cu:His_3Asp1-Aβ40 peptide than the apo-Aβ40 and other two Cu(II)-bound Aβ40 peptides.

Table 6. Formed Salt Briges of the apo and Cu(II)-bound Aβ40 Peptides. The probabilities of salt bridges formations in the structures of Aβ40, Cu(II):His_3Asp1-Aβ40, Cu(II):His_3Glu11-Aβ40, and Cu(II):His_3Tyr10-Aβ40 with a probability of greater than 10%. *R*(Cγ-Nζ) is the distance between the carboxylate carbon atom and the side-chain or N-terminal nitrogen atom.

Donor	Acceptor	Apo-Aβ40	Cu(II):His_3Asp1-Aβ40 R(C^{γ}-N^{ζ})	Cu(II):His_3Glu11-Aβ40 R(C^{γ}-N^{ζ})	Cu(II):His_3Tyr10-Aβ40 R(C^{γ}-N^{ζ})
Arg5	**Glu3**	67.83	0.08	66.92	73.04
Lys16	**Val40(-COO^-)**	36.84	0.53	3.54	1.73
Arg5	**Glu22**	35.27	9.39	5.97	19.95
Arg5	**Asp1**	26.75	-	16.3	16.51
Arg5	**Glu11**	25.28	22.71	-	11.08
Lys16	**Glu11**	17.25	10.33	-	0
Arg5	**Val40(-COO^-)**	15.21	41.63	29.74	11.69
Lys28	**Glu22**	11.36	3.82	3.47	4.17
Lys28	**Asp23**	3.98	3.57	1.32	13.47
Arg5	**Asp23**	0	22.92	30.99	0.06
Asp1(-$NH3^+$)	**Glu22**	0	13.28	0.28	0.06

The formed salt bridges of the apo- and Cu(II)-bound Aβ42 peptides also present the impact of Cu(II) coordination on the tertiary structure formations of Aβ42 with varying coordination chemistries (Table 7). These probabilities of salt bridge formation reveal that the salt bridge between between Arg5 and Glu22 is both significantly increased upon Cu(II) binding for all three coordination sites. Furthermore, the salt bridge formation between Arg5 and Asp1 increases for both Cu:His_3Glu11-Aβ42 and Cu:His_3Tyr10-Aβ42 as to apo-Aβ42. Cu:His_3Tyr10-Aβ42 displays less abundant Arg5 and Glu11 salt bridge formations than the other two Cu(II)-bound Aβ42 peptides and the apo-Aβ42 peptide. However, salt bridge formation between Arg5 and the C-terminus is increased for Cu:His_3Tyr10-Aβ42 as to apo-Aβ42 and other two Cu(II)-bound Aβ42. These findings are the vice versa trend of that reported for the apo- and Cu(II)-coordinated Aβ40 peptides (see above). However, we also observe specific trends that depend on the coordination chemistry that are similar to the of the apo and Cu(II)-bound Aβ peptides. For example, the salt bridges between Arg5 and Glu3 in only the Cu:His_3Asp1-Aβ42 peptide and between Arg5 and Glu11 in only the Cu:His_3Glu11-Aβ42 peptide are significantly decreased. Last, we note that Lys28 and Glu22 salt bridge probability in the Cu:His_3Tyr10-Aβ42 peptide and between Arg5 and Asp7 in the Cu:His_3Asp1-Aβ42 peptide is increased in comparison to the other three peptides.

Due to the proposed importance of aggregation to the pathogenic mechanism of AD, it is of great importance to be able to assess the affect of varying of copper ion coordination chemistries on the aggregation propensity Aβ. Pawar et al. developed a method to assess the residual aggregation propensity of IDPs (see Methods section) and applied it to Aβ peptides and other IDPs in order to assess where in the protein mutations affect the aggregation propensity (114). Using this method, we have calculated the residual intrinsic aggregation propensities (Z_{agg}) of the free and Cu(II)-coordinated Aβ alloforms utilizing the residual α-helix and β-sheet propensities obtained from our REMD simulations (Figures 7A and 7B). Pawar et al. presented that a Z_{agg} score of one or more indicates a high propensity to aggregate (114). Residues Phe4, Tyr10, Val12, Leu17, Phe19, Phe20, Val24, Ala30-Ile32, Leu34-Val36, and Val39-Val40 show the highest propensity to aggregate for the apo-Aβ40 peptide. Upon Cu(II), we note that the aggregation propensity of residues Leu17-Phe20 in the CHC region presents a notable increase in intrinsic aggregation propensity. Thus, this result indicates that the CHC region of the Cu(II)-bound Aβ40 peptides might be a key in their aggregation mechanism. Furthermore, intrinsic aggregation propensity for the CHC region residues is slightly higher for Cu:His_3Asp1-Aβ40 and Cu:His_3Glu11-Aβ40 as to Cu:His_3Tyr10-Aβ40. For apo-Aβ42, residues Phe4, Tyr10, Val12, Leu17, Phe19-Ala21, Val24, Ile31, Ile32, Leu34, Val36, and Val39-Ile41 display an intrinsic aggregation

propensity greater than one. Similar to the Aβ40 alloform, residues Leu17-Phe20 present an increase in intrinsic aggregation propensity upon Cu(II) binding regardless of the coordination chemistry, with the Cu:His_3Tyr10-Aβ42 peptide showing a lower increase than the Cu:His_3Asp1-Aβ42 and Cu:His_3Glu11-Aβ42 peptides. Additionally, we observe an increase in intrinsic aggregation propensity for residues Ile31-Met35 for the Cu:His_3Glu11-Aβ42 and Cu:His_3Tyr10-Aβ42 peptides in comparison to the apo-Aβ42 peptide. These findings indicate that the CHC and C-terminal regions are also involved in the aggregation mechanism of Cu(II)-coordinated Aβ42 but the level of aggregation propensity may vary based on the differences in the coordination chemistry of the Cu(II) ion. See also, Tables S1 and S2 in the supporting information section.

Table 7. Formed Salt Briges of the apo and Cu(II)-bound Aβ42 Peptides. The probabilities of salt bridges formations in the structures of Aβ42, Cu(II):His_3Asp1-Aβ42, Cu(II):His_3Glu11-Aβ42, and Cu(II):His_3Tyr10-Aβ42 with a probability of greater than 10%. *R*(Cγ-Nζ) is the distance between the carboxylate carbon atom and the side-chain or N-terminal nitrogen atom.

Donor	Acceptor	Apo-Aβ42	Cu(II):His_3Asp1-Aβ42 R(C^{γ}-N^{ζ})	Cu(II):His_3Glu11-Aβ42 R(C^{γ}-N^{ζ})	Cu(II):His_3Tyr10-Aβ42 R(C^{γ}-N^{ζ})
Arg5	**Glu3**	61.9	1.1	65.6	41.9
Arg5	**Glu11**	37.5	39.0	-	2.7
Arg5	**Ala42(-COO^-)**	18.0	16.8	14.2	30.7
Arg5	**Asp1**	17.8	-	27.1	23.3
Arg5	**Asp23**	14.9	7.5	7.1	9.9
Arg5	**Glu22**	5.6	20.9	24.5	19.2
Lys28	**Glu22**	3.1	3.3	2.5	13.0
Arg5	**Asp7**	0.1	33.3	0.3	12.1

Figure 7A. Residual intrinsic aggregation scores (Zagg) of the apo and Cu(II)-bound Aβ40 Peptides. Calculated Zagg values for each residue of the Aβ40, Cu(II):His_3Asp1-Aβ40, Cu(II):His_3Glu11-Aβ40, and Cu(II):His_3Tyr10-Aβ40 peptides in an aqueous solution.

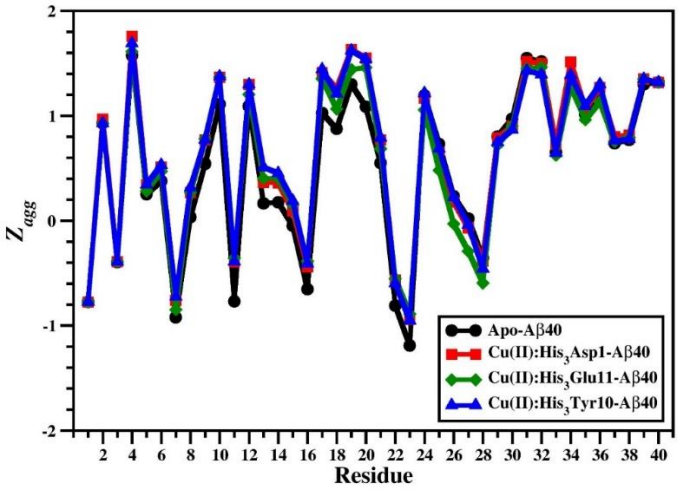

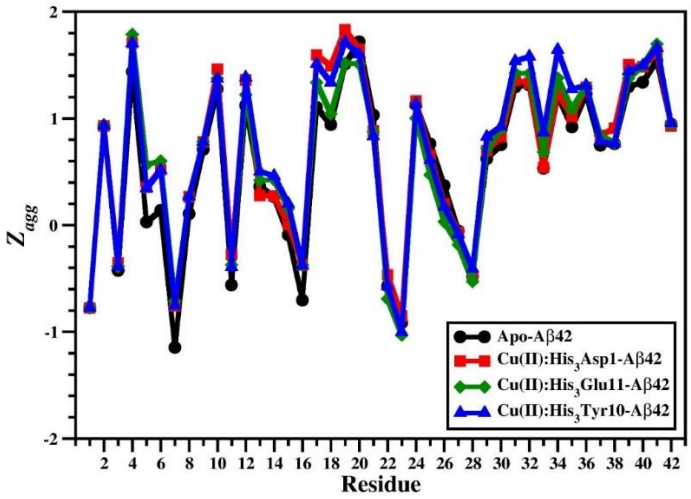

Figure 7B. Residual intrinsic aggregation scores (Z_{agg}) of the apo and Cu(II)-bound Aβ42 Peptides. Calculated Z_{agg} values for each residue of the Aβ42, Cu(II):His$_3$Asp1-Aβ42, Cu(II):His$_3$Glu11-Aβ42, and Cu(II):His$_3$Tyr10-Aβ42 peptides in an aqueous solution.

CONCLUSIONS

Overall, results show the specific structural and thermodynamic properties of aqueous Cu(II)-bound Aβ40 and Aβ42 peptides with different Cu(II) coordination chemistries. Furthermore, the affect of Cu(II) coordination on Aβ40 and Aβ42 peptides and the alloform specific differences in Cu(II)-bound Aβ including coordination specific differences is presented. The results presented herein are the first to offer a comparison of the monomeric Cu(II)-coordinated Aβ40 and Aβ42 peptides for these three different proposed species I binding sites including three histidine residues utilizing the new potential functions. Furthermore, this study presents the usefulness of our developed force field parameters for type II copper centers in proteins including three His residues (84).

In summary, the thermodynamic properties of apo- and Cu(II)-bound Aβ40 and Aβ42 present that the Cu(II)-bound structures are less preferred than apo-Aβ40 and apo-Aβ42 in aqueous solution. In addition, both Aβ alloforms display a difference in the favorability of the structures based on the coordination chemistry. Specifically, thermodynamic preference for the coordination sites is Cu:His$_3$Glu11 < Cu:His$_3$Tyr10 < Cu:His$_3$Asp1 for both Aβ alloforms. The PMF surfaces of the free and Cu(II)-bound Aβ peptides also reveal that the conformational ensemble of the Aβ peptides is altered by Cu(II) coordination and that the change in the conformational ensemble differs based on the chosen binding site.

In general, the helical content of the Cu(II)-bound alloforms decreases in the N-terminal and CHC regions for all three coordination chemistries except for the 3_{10}-helical content for Val12-Gln15 in the Cu:His$_3$Glu11-Aβ40 and Cu:His$_3$Glu11-Aβ42 peptides. The β-sheet content is decreased for the Aβ40 peptide upon Cu(II) binding except within residues Leu34-Val40 residing in the C-terminal region. Conversely, the Aβ42 peptide shows a boost in β-sheet content in the CHC and C-terminal regions for all three binding sites and an increase in the N-terminal region for the Cu:His$_3$Glu11 binding site. Furthermore, the increased structuring in the C-terminal region of the free Aβ42 in comparison to the free Aβ40 is still observed when Cu(II) binds to the peptide. Additionally, increased structuring in the CHC region due to β-sheet formation for the Cu(II)-bound Aβ42 peptides as to the Cu(II)-bound Aβ40 peptides is also observed. Altogether, these β-sheet content variations indicate that the Cu(II)-coordinated Aβ peptides have an increased aggregation rate in comparison to the free Aβ peptides and that the Cu(II)-bound Aβ42 peptides will aggregate more rapidly than the Cu(II)-bound Aβ40 peptides. The calculated tertiary structures also reveal differences due to Cu(II)-binding including the impact of the chosen coordination chemistry and alloform specific differences of the Cu(II)-bound Aβ peptides. Namely, intra-molecular interactions within the C-terminal region decrease when Cu(II) binds to the Aβ40 peptide. In addition, N- and C-terminal regions as well as CHC and N-terminal regions interactions are shifted upon Cu(II) binding to Aβ40 and Aβ42. Furthermore, alloform specific changes are also observed, indicating that the change in the conformational ensemble of the Aβ peptides depends on the coordination chemistry. Therefore, these different structural effects resulting from the different binding sites might help to elucidate the

coordination chemistry of the Aβ peptide under different solution conditions.

Intrinsic aggregation propensity calculation reveal that the CHC and C-terminal regions are most likely to be involved in the aggregation of the free and Cu(II)-bound Aβ40 and Aβ42 peptides in aqueous solution. Furthermore, the Cu(II) binding enhances the intrinsic aggregation of the CHC region for the Aβ40 peptide and of the CHC and C-terminal regions for the Aβ42 peptide. However, we should note that the α parameters for the intrinsic aggregation propensity equation were optimized based on aggregation information of the free and mutant-type Aβ peptides. Therefore, further optimization might be required to account for changes in the aggregation rate due to transition metal ion binding. In addition, the values typically used for this equation are based on general hydrophobicity, α-helix and β-sheet content information for individual amino acid residues. Therefore, further optimization may be required to include information from molecular dynamics simulations, such as the non-polar solvent accessible surface area. Finally, the results presented herein can provide potential targets for the development of aggregation inhibitors of Cu(II)-bound Aβ peptides as well as structural information that can be used to aid in differentiating the Cu(II) coordination chemistry for the Aβ peptides under different solution conditions once detailed structural information can be obtained from experimental measurements of the Cu(II)-bound Aβ peptides in aqueous solution.

ACKNOWLEDGMENTS

The author thanks O. Wise (The University of Texas at San Antonio) for helpful discussions.

REFERENCES

1. Faller P, Hureau C. Bioinorganic chemistry of copper and zinc ions coordinated to amyloid-beta peptide. Dalton Trans. 2009 Feb;21:1080-1094.

2. Atwood C. S, Moir R. D, Huang X. D, Scarpa R. C, Bacarra N. M, Romano D. M, Hartshorn M. K, Tanzi R. E, Bush A. I. Dramatic aggregation of Alzheimer Aβ by Cu(II) is induced by conditions representing physiological acidosis. J. Biol. Chem. 1998 May;273:12817-12826.

3. Zou J, Kajita K, Sugimoto N. Cu2+ inhibits the aggregation of amyloid beta-peptide(1-42) in vitro. Angew. Chem. Int. Ed. 2001 Jun; 40:2274-2277.

4. Raman B, Ban T, Yamagucchi K, Sakai M. Kawai T, Naiki H, Goto Y. Metal ion-dependent effects of clioquinol on the fibril growth of an amyloid beta peptide. J. Biol. Chem. 2005 Apr; 280:16157-16162.

5. House E, Collingwood J, Khan A, Korchazkina O, Berthon G, Exley C. Aluminium, iron, zinc and copper influence the in vitro formation of amyloid fibrils of A beta(42) in a manner which may have consequences for metal chelation therapy in Alzheimer's disease. J. Alz. Dis. 2004 Jun;6:291-301.

6. Yang X-H, Huang H-C, Chen L, Xu W, Jiang Z-F. Coordinating to Three Histidine Residues: Cu (II) Promotes Oligomeric and Fibrillar Amyloid-β Peptide to Precipitate in a Non-β Aggregation Manner. J. Alz. Dis. 2009 Nov;18:799-810.

7. Yu H, Ren J, Qu X. Different Hydration Changes Accompanying Copper and Zinc Binding to Amyloid β-Peptide: Water Contribution to Metal Binding. ChemBioChem. 2008 Feb;9:879-882.

8. Dai X, Sun Y, Gao Z, Jiang Z. Copper enhances amyloid-β peptide neurotoxicity and non β-aggregation: a series of experiments conducted upon copper-bound and copper-free amyloid-β peptide. J. Mol. Neurosci. 2010 May;41:66-73.

9. Hou L, Zagorski M G. NMR reveals anomalous copper(II) binding to the amyloid A beta peptide of Alzheimer's disease. J. Am. Chem. Soc. 2006 Jun;128:9260-9261.

10. Yoshiike Y, Tanemura K, Murayama O, Akagi T, Murayama M, Sato S, Sun X Y, Tanaka N, Takashima A. New insights on how metals disrupt amyloid beta-aggregation and their effects on amyloid-beta cytotoxicity. J. Biol. Chem. 2001 Aug; 276:32293-32299.

11. Smith D. P, Ciccotosto G. D, Tew D. J, Fodero-Tavoletti M. T, Johanssen T, Masters C. L, Barnham K. J, Cappai R. Concentration dependent Cu2+ induced aggregation and dityrosine formation of the Alzheimer's disease Amyloid-β peptide Biochem. 2007 Mar;46:2881-2891.

12. Jun S, Saxena S. The aggregated state of amyloid-beta peptide in vitro depends on Cu2+ ion concentration. Angew. Chem. Int. Edit. 2007 May;46:3959-3961.

13. Bolognin S, Messori L, Drago D, Gabbiani C, Cendron L, Zatta P. Aluminum, copper, iron and zinc differentially alter amyloid-Aβ< sub>

1–42</sub> aggregation and toxicity. Int. J Biochem. & Cell Biol. 2011 Jun;43:877-885.

14. Mold M, Ouro-Gnao L, Wieckowski B. M, Exley C. Copper prevents amyloid-[bgr] 1-42 from forming amyloid fibrils under near-physiological conditions in vitro. Scientific Reports. 2013 Feb;3:1256.

15. Hane F, Tran G, Attwood S. J, Leonenko Z. Cu2+ affects amyloid-β (1–42) aggregation by increasing peptide-peptide binding forces. PloS one. 2013 Mar;8:e59005.

16. Attanasio F, De Bona P, Cataldo S, Sciacca M. F. M, Milardi D, Pignataro B, Pappalardo G. Copper(II) and zinc(II) dependent effects on A beta 42 aggregation: a CD, Th-T and SFM study. New J. Chem. 2013 37(4):1206-1215.

17. Huang X. D, Atwood C. S, Moir R. D, Hartshorn M. A, Tanzi R. E, Bush A. I. Trace metal contamination initiates the apparent auto-aggregation, amyloidosis, and oligomerization of Alzheimer's A beta peptides. J. Biol. Inorg. Chem. 2004 Dec;9:954-960.

18. Karr J. W, Szalai V. A. Role of aspartate-1 in Cu(II) binding to the amyloid-β peptide of Alzheimer's disease. J. Am. Chem. Soc. 2007 Mar;129:3796-3797.

19. Karr J. W, Kaupp L. J, Szalai V. A. Amyloid-beta binds Cu2+ in a mononuclear metal ion binding site. J. Am. Chem. Soc. 2004 Oct;126:13534-13538.

20. Sarell C. J, Wilkinson S. R, Viles J. H. Substoichiometric Levels of Cu2+ Ions Accelerate the Kinetics of Fiber Formation and Promote Cell Toxicity of Amyloid-beta from Alzheimer Disease. J. Biol. Chem. 2010 Dec;285:41533-41540.

21. Jun S, Gillespie J. R, Shin B.-k, Saxena S. The Second Cu(II)-Binding Site in a Proton-Rich Environment Interferes with the Aggregation of Amylold-beta(1-40) into Amyloid Fibrils. Biochem. 2009 Oct;48:10724-10732.

22. Lv Z, Condron M. M, Teplow D. B, Lyubchenko Y. L. Nanoprobing of the Effect of Cu 2D Cations on Misfolding, Interaction and Aggregation of Amyloid Beta Peptide. Biophys. J. 2013 Jan;104:513A-514A.

23. Bush A. I. The metallobiology of Alzheimer's disease. Trends in Neurosciences. 2003 Apr;26:207-214.

24. Opazo C, Huang X. D, Cherny R. A, Moir R. D, Roher A. E, White A. R, Cappai R, Masters C. L, Tanzi R. E, Inestrosa N. C, Bush A. I. Metalloenzyme-like activity of Alzheimer's disease beta-amyloid - Cu-dependent catalytic conversion of dopamine, cholesterol, and biological reducing agents to neurotoxic H2O2. J. Biol. Chem. 2002 Oct;277:40302-40308.

25. Cuajungco M. P, Faget K. Y. Zinc takes the center stage: its paradoxical role in Alzheimer's disease. Brain Res. Rev. 2003 Jan;41:44-56.

26. Huang X. D, Atwood C. S, Hartshorn M. A, Multhaup G, Goldstein L. E, Scarpa R. C, Cuajungco M. P, Gray D. N, Lim, J, Moir R. D, Tanzi R. E, Bush A. I. The A beta peptide of Alzheimer's disease directly produces hydrogen peroxide through metal ion reduction. Biochem. 1999 May;38:7609-7616.

27. Sharma A. K, Pavlova S. T, Kim J, Kim J, Mirica L. M. The effect of Cu2+ and Zn2+ on the A beta(42) peptide aggregation and cellular toxicity. Metallomics. 2013 Nov;5:1529-1536.

28. Huang X. D, Cuajungco M. P, Atwood C. S, Hartshorn M. A, Tyndall J. D. A, Hanson G. R, Stokes K. C, Leopold M, Multhaup G, Goldstein L. E, Scarpa R. C, Saunders A. J, Lim J, Moir R. D, Glabe C, Bowden E. F, Masters C. L, Fairlie D. P, Tanzi R. E, Bush A. I. Cu(II) potentiation of Alzheimer A beta neurotoxicity - Correlation with cell-free hydrogen peroxide production and metal reduction. J. Biol. Chem. 1999 Dec;274:37111-37116.

29. Nadal R. C, Rigby S. E. J, Viles J. H. Amyloid beta-Cu2+ Complexes in both Monomeric and Fibrillar Forms Do Not Generate H2O2 Catalytically but Quench Hydroxyl Radicals. Biochem. 2008 Nov;47:11653-11664.

30. Fang C.-L, Wu W.-H, Liu Q, Sun X. Ma Y, Zhao Y.-F, Li Y.-M. Dual functions of beta-amyloid oligomer and fibril in Cu(II)-induced H2O2 production. Regulatory Peptides. 2010 May;163:1-6.

31. Garzon-Rodriguez W, Yatsimirsky A. K, Glabe C. G. Binding of Zn(II), Cu(II), and Fe(II) ions to Alzheimer's A beta peptide studied by fluorescence. Bioorganic & Medicinal Chemistry Letters. 1999 Aug;9:2243-2248.

32. Atwood C. S, Scarpa R. C, Huang X. D, Moir R. D, Jones W. D, Fairlie D. P, Tanzi R. E, Bush A. I. Characterization of copper interactions with Alzheimer amyloid beta peptides: Identification of an attomolar-affinity copper binding site on amyloid beta 1-42. J. Neurochem. 2008 Sep;75:1219-1233.

33. Guilloreau L, Damian L, Coppel Y, Mazarguil H, Winterhalter M, Faller P. Structural and thermodynamical properties of CuII amyloid-β 16/28 complexes associated with Alzheimer's disease. J. Biol. Inorg. Chem. 2006 Aug;11:1024-1038.

34. Jiang D, Men L, Wang J, Zhang Y, Chickenyen S, Wang Y, Zhou F. Redox reactions of copper complexes formed with different beta-amyloid peptides and their neuropathalogical relevance. Biochem. 2007 Jul;46:9270-9282.

35. Karr J. W, Szalai V. A. Cu(II) binding to monomeric, oligomeric, and fibrillar forms of the Alzheimer's disease amyloid-beta peptide. Biochem. 2008 Apr;47:5006-5016.

36. Syme C. D, Nadal R. C, Rigby S. E. J, Viles J. H. Copper binding to the amyloid-beta (A beta) peptide associated with Alzheimer's disease - Folding, coordination geometry, pH dependence, stoichiometry, and affinity of A beta-(1-28): Insights from a range of complementary spectroscopic techniques. J. Biol. Chem. 2004 Apr;279:18169-18177.

37. Danielsson J, Pierattelli R, Banci L, Graslund A. High-resolution NMR studies of the zinc-binding site of the Alzheimer's amyloid beta-peptide. Febs J. 2007 Nov;274:46-59.

38. Bush A. I, Pettingell W. H, Multhaup G, Paradis M. D, Vonsattel J. P, Gusella J. F, Beyreuther K, Masters C. L, Tanzi R. E. Rapid Induction of Alzheimer a-Beta Amyloid Formation by Zinc. Science. 1994 Sep;265:1464-1467.

39. Tougu V, Karafin A, Palumaa P. Binding of zinc(II) and copper(II) to the full-length Alzheimer's amyloid-beta peptide. J. Neurochem. 2008 Mar;104:1249-1259.

40. Hatcher L. Q, Hong L, Bush W. D, Carducci T, Simon J. D. Quantification of the binding constant of copper(II) to the amyloid-beta peptide. J. Phys. Chem. B. 2008 Jul;112:8160-8164.

41. Karr J. W, Akintoye H, Kaupp L. J, Szalai V. A. N-terminal deletions modify the Cu2+ binding site in amyloid-beta. Biochem. 2005 Mar;44:5478-5487.

42. Kowalik-Jankowska T, Ruta M, Wisniewska K, Lankiewicz L. Coordination abilities of the 1-16 and 1-28 fragments of beta-amyloid peptide towards copper(II) ions: a combined potentiometric and spectroscopic study. J. Inorg. Biochem. 2003 Jul;95:270-282.

43. Ma Q.-F, Hu J, Wu W.-H, Liu H.-D, Du J.-T, Fu Y, Wu Y.-W, Lei P, Zhao Y.-F, Li Y.-M. Characterization of copper binding to the peptide amyloid-beta(1-16) associated with Alzheimer's disease. Biopolymers. 2006 Apr;83:20-31.

44. Hong L, Bush W. D, Hatcher L. Q, Simon J. Determining thermodynamic parameters from isothermal calorimetric isotherms of the binding of macromolecules to metal cations originally chelated by a weak ligand. J. Phys. Chem. B. 2008 Nov;112:604-611.

45. Curtain C. C, Ali F, Volitakis I, Cherny R. A, Norton R. S, Beyreuther K, Barrow C. J, Masters C. L, Bush A. I, Barnham K. J. Alzheimer's disease amyloid-beta binds copper and zinc to generate an allosterically ordered membrane-penetrating structure containing superoxide dismutase-like subunits. J. Biol. Chem. 2001 Jun;276:20466-20473.

46. Minicozzi V, Stellato F, Comai M, Dalla Serra M, Potrich C, Meyer-Klaucke W, Morante S. Identifying the minimal copper- and zinc-binding site sequence in amyloid-beta peptides. J. Biol. Chem. 2008 Apr;283:10784-10792.

47. Miura T, Suzuki K, Kohata N, Takeuchi H. Metal binding modes of Alzheimer's amyloid beta-peptide in insoluble aggregates and soluble complexes. Biochem. 2000 May;39:7024-7031.

48. Stellato F, Menestrina G, Dalla Serra M, Potrich C, Tomazzolli R, Meyer-Klaucke W, Morante S. Metal binding in amyloid β-peptides shows intra- and inter-peptide coordination modes. Eur. Biophys. J. 2006 Jan;35:340-351.

49. Ma Q. F, Hu J, Wu W. H, Liu H. D, Du J. T, Fu Y, Wu Y. W, Lei P, Zhao Y. F, Li Y. M. Characterization of copper binding to the peptide amyloid-beta(1-16) associated with Alzheimer's disease. Biopoly. 2006 Apr;83:20-31.

50. Streltsov V. A, Titmuss S. J, Epa V. C, Barnham K. J, Masters C. L, Varghese J. N. The structure of the amyloid-beta peptide high-affinity copper II binding site in Alzheimer disease. Biophys. J. 2008 Oct;95:3447-3456.

51. Drew S. C, Noble C. J, Masters C. L, Hanson G. R, Barnham K. J. Pleomorphic Copper Coordination by Alzheimer's Disease Amyloid-beta Peptide. J. Am. Chem. Soc. 2009 Jan;131:1195-1207.

52. Kowalik-Jankowska T, Ruta-Dolejsz M, Wisniewska K, Lankiewicz L. Cu(II) interaction with N-terminal fragments of human and mouse beta-amyloid peptide. J. Inorg. Biochem. 2001 Sep;86:535-545.

53. Curtain C. C, Ali F. E, Smith D. G, Bush A. I, Masters C. L, Barnham K. J. Metal ions, pH, and cholesterol regulate the interactions of Alzheimer's disease amyloid-beta peptide with membrane lipid. J. Biol. Chem. 2003 Jan;278:2977-2982.

54. Shin B.-k, Saxena S. Direct evidence that all three histidine residues coordinate to Cu(II) in amyloid-beta(1-16). Biochem. 2008 Sep;47:9117-9123.

55. Barnham K. J, Haeffner F, Ciccotosto G. D, Curtain C. C, Tew D, Mavros C, Beyreuther K, Carrington D, Masters C. L, Cherny R. A, Cappai R, Bush A. I. Tyrosine gated electron transfer is key to the toxic mechanism of Alzheimer's disease beta-amyloid. Faseb J. 2004 Jul;18:1427-1428.

56. Liao Q, Kammerlin S. C. L, Strodel B. Development and application of a nonbonded Cu(II) model that includes Jahn-Teller effect. Phys. Chem. Lett. 2015 Jun; 6:2657-2662.

57. Liao Q, Owen M. C., Olubiyi O. O, Bogdan B, Strodel B. Conformational Transitions of the Amyloid-β Peptide Upon Cu(II) Binding and pH Changes. Isr. J. Chem. 2017; 57:1-15.

58. Liao Q, Owen M. C, Bali S, Barz B, Strodel B. Aβ under stress: the effects of acidosis, Cu(II) binding, and oxidation on amyloid-β peptide dimers. Chem Commun. 2018 Jun; 54:7766-7769.

59. Ando K. The axial methionine ligand may control the redox reorganizations in the active site of blue copper proteins. J. Chem. Phys. 2010 Nov;133:0175101.

60. Bruschi M, Bertini L, Bonacic-Koutecky V, De Gioia L, Mitric R, Zampella G, Fantucci P. Speciation of Copper-Peptide Complexes in Water Solution Using DFTB and DFT Approaches: Case of the Cu(HGGG)(Py) Complex. J. Phys. Chem. B. 2012 Jun;116:6250-6260.

61. Hewitt N, Rauk A. Mechanism of Hydrogen Peroxide Production by Copper-Bound Amyloid Beta Peptide: A Theoretical Study. J. Phys. Chem. B. 2009 Jan;113:1202-1209.

62. Hodak M, Chisnell R, Lu W, Bernholc J. Functional implications of multistage copper binding to the prion protein. Proc. Nat. Acad. Sci. USA 2009 Jul;106:11576-11581. DOI: 10.1073/pnas.0903807106.

63. Inoue T, Shiota Y, Yoshizawa K. Quantum Chemical Approach to the Mechanism for the Biological Conversion of Tyrosine to Dopaquinone. J. Am. Chem. Soc. 2008 Nov;130:16890-16897.

64. Kaila V. R. I, Johansson M. P, Sundholm D, Laakkonen L, Wikstrom M. The chemistry of the Cu-B site in cytochrome c oxidase and the importance of its unique His-Tyr bond. Biochim. Biophys. Acta-Bioenergetics. 2009 Apr;1787:221-233.

65. Konecny R, Li J, Fisher C. L, Dillet V, Bashford D, Noodleman L. CuZn superoxide dismutase geometry optimization, energetics, and redox potential calculations by density functional and electrostatic methods. Inorg. Chem. 1999 Feb;38:940-950.

66. Pavelka M, Simanek M, Sponer J, Burda J. V. Copper cation interactions with biologically essential types of ligands: A computational DFT study. J. Phys. Chem. A. 2006 Mar;110:4795-4809.

67. Prabhakar R, Siegbahn P. E. M. A theoretical study of the mechanism for the biogenesis of cofactor topaquinone in copper amine oxidases. J. Am. Chem. Soc. 2004 Mar;126:3996-4006.

68. Rickard G. A, Gomez-Balderas R, Brunelle P, Raffa D. F, Rauk A. Binding affinities for models of biologically available potential Cu(II) Ligands relevant to Alzheimer's disease: An ab initio study. J. Phys. Chem. A. 2005 Aug;109:8361-8370.

69. Rimola A, Rodriguez-Santiago, L, Sodupe M. Cation-pi interactions and oxidative effects on Cu+ and Cu2+ binding to Phe, Tyr, Trp, and his amino acids in the gas phase. Insights from first-principles calculations. J. Phys. Chem. B. 2006 Nov;110:24189-24199.

70. Rokhsana D, Dooley D. M, Szilagyi R. K. Structure of the oxidized active site of galactose oxidase from realistic in silico models. J. Am. Chem. Soc. 2006 Nov;128:15550-15551.

71. Rokhsana D, Howells A. E, Dooley D. M, Szilagyi R. K. Role of the Tyr-Cys Cross-link to the Active Site Properties of Galactose Oxidase. Inorg. Chem. 2012 Feb;51:3513-3524.

72. Sabolovic J, Tautermann C. S, Loerting T, Liedl K. R. Modeling anhydrous and aqua copper(II) amino acid complexes: A new

molecular mechanics force field parametrization based on quantum chemical studies and experimental crystal data. Inorg. Chem. 2003 Mar;42:2268-2279.

73. Blomberg M. R. A, Siegbahn P. E. M. Quantum chemistry applied to the mechanisms of transition metal containing enzymes - Cytochrome c oxidase, a particularly challenging case. J. Comp. Chem. 2006 Jun;27:1373-1384.

74. Hong G, Ivnitski D. M, Johnson G. R, Atanassov P, Pachter R. Design Parameters for Tuning the Type 1 Cu Multicopper Oxidase Redox Potential: Insight from a Combination of First Principles and Empirical Molecular Dynamics Simulations. J. Am. Chem. Soc. 2011 Apr;133(13):4802-4809.

75. Moon S, Patchkovskii S, Salahub D. R. QM/MM calculations of EPR hyperfine coupling constants in blue copper proteins. J. Mol. Struct.-Theochem. 2003 Aug;632:287-295.

76. Rodriguez-Granillo A, Crespo A, Wittung-Stafshede P. Conformational Dynamics of Metal-Binding Domains in Wilson Disease Protein: Molecular Insights into Selective Copper Transfer. Biochem. 2009 Jun;48:5849-5863.

77. Rose F, Hodak M, Bernholc J. Mechanism of copper(II)-induced misfolding of Parkinson's disease protein. Scientific Reports. 2011 Jun;1:11.

78. Sinnecker S, Neese F. QM/MM calculations with DFT for taking into account protein effects on the EPR and optical spectra of metalloproteins. Plastocyanin as a case study. J. Comput. Chem. 2006 Jun;27:1463-1475.

79. Brancato G, Rega N, Barone V. Microsolvation of the Zn(II) ion in aqueous solution: A hybrid QM/MM MD approach using non-periodic boundary conditions. Chem. Phys. Lett. 2008 Dec;451:53-57.

80. Hartsough D. S. Merz K. M. Dynamic Force Field Models – Molecular-Dynamics Simulations of Human Carbonic-Anhydrase-II Using a Quantum-Mechnaical Molecular Mechanical Coupled Potential. J Phys Chem. 1995 Jul;99:11266-11275.

81. Ryde, U. The coordination of the catalytic zinc ion in alcohol dehydrogenase studied by combined quantum-chemical and molecular mechanics calculations. J. Computer-Aided Molecular Design. 1996 Jan;10(2):153-164.

82. Ryde U. Combined quantum and molecular mechanics calculations on metalloproteins" Current Opinion in Chemical Biology. 2003 Feb;7:136-142.

83. Mutter S. T, Deeth R. J, Turner M, Platts J. A. Benchmarking of copper(II) LFMM parameters for studying amyloid-β peptides. J. Biomol. Struct. Dyn. 2017 Apr;36:1145-1153.

84. Wise O, Coskuner O. New force field parameters for metalloproteins I: Divalent copper ion centers including three histidine residues and an oxygen-ligated amino acid residue. J. Comput. Chem. 2014 Apr;35:1278-1289.

85. Coskuner O. Divalent copper ion bound amyloid-β(40) and amyloid-β(42) alloforms are less preferred than divalent zinc ion bound amyloid-β(40) and amyloid-β(42) alloforms. J. Biol. Inorg. Chem. 2016 Sept;21:957.

86. Coskuner Weber O, Uversky V. N. How accurate are your simulations? Effects of confined aqueous volume and AMBER FF99SB and CHARMM22/CMAP force field parameters on structural ensembles of intrinsically disordered proteins: Amyloid-β42 in water. Intrinsically Disordered Proteins. 2017 Oct;5:1.

87. Xu L, Wang X, Shan S, Wang X. Characterization of the polymorphic states of copper(II)-bound Aβ(1–16) peptides by computational simulations. J. Comp. Chem. Aug;34:2524-2536.

88. Wise-Scira O, Xu L, Kitahara T, Perry G, Coskuner O. Amyloid-β peptide structure in aqueous solution varies with fragment size. J. Chem. Phys. 2011 Nov;135:205101.

89. Parthasarathy S, Long F, Miller Y, Xiao Y, McElheny D, Thurber K, Ma, Nussinov R, Ishii Y. Molecular-Level Examination of Cu2+ Binding Structure for Amyloid Fibrils of 40-Residue Alzheimer's β by Solid-State NMR Spectroscopy. J. Am. Chem. Soc. 2011 Feb;133:3390-3400.

90. Domingo A, Angeli C, de Graaf C, Robert V. Electronic reorganization triggered by electron transfer: The intervalence charge transfer of a Fe3+/Fe2+ bimetallic complex. J. Comp. Chem. 2015 Mar;36:861-869.

91. Bixon M, Jortner J. Electron Transfer – from Isolated Molecules to Biomolecules. 1999. John Wiley & Sons. ISBN: 9780471252924.

92. Coskuner O, Bergeron D. E, Rincon L, Hudgens J. W, Gonzalez C. A. Identification of

Active Sites of Biomolecules. 1. Methyl-α-mannopyranoside and FeIII. J. Phys. Chem. A 2008 Feb;112:2940-2947.

93. Coskuner O, Bergeron D. E, Rincon L, Hudgens J. W, Gonzalez C. A. Identification of active sites of biomolecules II: Saccharide and transition metal ion in aqueous solution. J. Phys. Chem. A 2009 Feb;113:2491-2499.

94. Kodali R, Williams A. D, Chemuru S, Wetzel R. Aβ(1–40) Forms Five Distinct Amyloid Structures whose β-Sheet Contents and Fibril Stabilities Are Correlated. J. Mol. Biol. 2010 Aug;401:503-517.

95. Tycko R, Wickner R. B. Molecular structures of amyloid and prion fibrils: consensus versus controversy. Acc. Chem. Res. 2013 Jul;46:1487-1496.

96. Wise-Scira O, Xu L, Perry G, Coskuner O. Structures and free energy landscapes of aqueous zinc(II)-bound amyloid-β(1–40) and zinc(II)-bound amyloid-β(1–42) with dynamics. J. Biol. Inorg. Chem. 2012 Jun;17:927-938.

97. Sharma A. K, Pavlova S. T, Kim J, Finkelstein D, Hawco N. J, Rath N. P, Kim J, Mirica L. M. Bifunctional compounds for controlling metal-mediated aggregation of the aβ42 peptide. J. Am. Chem. Soc. 2012 Apr;134:6625-6636.

98. Asandei A, Schiopu I, Iftemi S, Mereuta L, Luchian T. Investigation of Cu2+ binding to human and rat amyloid fragments Aβ (1-16) with a protein nanopore. Langmuir 2013 Dec;29:15634-15642.

99. Morante S. The Role of Metals in β - Amyloid Peptide Aggregation: X-Ray Spectroscopy and Numerical Simulations. Curr. Alz. Res. 2008 Dec;5:508-524.

100. Silva K. I, Michael B. C, Geib S. J, Saxena S. ESEEM Analysis of Multi-Histidine Cu(II)-Coordination in Model Complexes, Peptides, and Amyloid-β. J. Phys. Chem. B 2014 Jul;118:8935-8944.

101. El Khoury Y, Dorlet P, Faller P, Hellwig P. New Insights into the Coordination of Cu(II) by the Amyloid-B 16 Peptide from Fourier Transform IR Spectroscopy and Isotopic Labeling. J. Phys. Chem. B 2011 Oct;115:14812-14821.

102. Hane F, Tran G, Attwood S. J, Leonenko Z. Cu(2+) affects amyloid-β (1-42) aggregation by increasing peptide-peptide binding forces. PLoS One 2013 Mar;8:e59005.

103. Nair N. G, Perry G, Smith M. A, Reddy V. P. NMR studies of zinc, copper, and iron binding to histidine, the principal metal ion complexing site of amyloid-beta peptide. J. Alz. Dis. 2010 Mar;20:57-66.

104. Allison T. C, Coskuner O, Gonzalez C. A. Metallic Systems: A Quantum Chemist´s Perspective. Boca Raton CRC Press/Taylor & Francis; 2011432 p. ISBN: 978-4200-6986-7.

105. Hornak V, Abel R, Okur A, Strockbine B, Roitberg A, Simmerling C. Comparison of multiple Amber force fields and development of improved protein backbone parameters. Proteins. 2006 Nov;65:712-725.

106. Binder K, Horbach J, Kob W, Paul W, Varnik F. Molecular dynamics simulations. J. Phys.: Cond. Matter 2004 Jan;16:S429-S453.

107. Beeman D. Some multistep methods for use in molecular dynamics calculations. J. Comput. Phys. 1976 Feb;20:130-139.

108. Xu L, Wang X, Wang X. Characterization of the internal dynamics and conformational space of zinc-bound amyloid β peptides by replica-exchange molecular dynamics simulations. 2013 July;42:575-586.

109. Xu L, Wang X, Wang X. Effects of Zn2+ Binding on the Structural and Dynamic Properties of Amyloid B Peptide Associated with Alzheimer's Disease: Asp1 or Glu11? 2013 Aug;4:1458-1468.

110. Prakash M. K, Barducci A, Parrinello M. Replica Temperatures for Uniform Exchange and Efficient Roundtrip Times in Explicit Solvent Parallel Tempering Simulations. J. Chem. Theory Comput. 2011 Jun;7:2025-2027.

111. Lee M. R, Duan Y, Kollman P. A. Use of MM-PB/SA in estimating the free energies of proteins: application to native, intermediates, and unfolded villin headpiece. Proteins. 2000 Jun;39:309-316.

112. Kollman P. A, Massova I, Reyes C, Kuhn B, Huo S, Chong L, Lee M, Lee T, Duan Y, Wang W, Donini O, Cieplak P, Srinivasan J, Case D. A, Cheatham T. E. Calculating Structures and Free Energies of Complex Molecules: Combining Molecular Mechanics and Continuum Models. Acc. Chem. Res. 2000 Oct;33:889-897.

113. Kabsch W, Sander C. Dictionary of protein secondary structure: pattern recognition of hydrogen-bonded and geometrical features. Biopolymers. 1983 Dec;22:2577-2637.

114. Pawar A. P, DuBay K. F, Zurdo J, Chiti F, Vendruscolo M, Dobson C. M. Prediction of "aggregation-prone" and "aggregation-susceptible" regions in proteins associated with neurodegenerative diseases. J. Mol. Biol. 2005 Jul;350:379-392.

115. Nagypal I, Gergely A, Farkas E. Thermodynamic Study of Parent and Mixed Complexes of Aspartic-acid, Glutamic-acid and Glycine with Copper(II). Journal of Inorganic & Nuclear Chemistry. 1974 ;36:699-706.

116. Gassmann E, Kuo J. E, Zare R. N. Electrokinetic Separation of Chiral Compounds. Science. 1985 Nov;230:813-814.

117. Gozel P, Gassmann E, Michelsen H, Zare R. N. Electrokinetic Resolution of Amino-Acid Enantiomers with Copper(II) Aspartame Support Electrolyte. Analytical Chemistry. 1987 Jan;59:44-49.

118. Rickard G. A, Gomez-Balderas R, Brunelle P, Raffa D. F, Rauk A. Binding affinities for models of biologically available potential Cu(II) Ligands relevant to Alzheimer's disease: An ab initio study. J. Phys. Chem. A. 2005 Sep;109:8361-8370.

119. Smith D. P, Smith D. G, Curtain C. C, Boas J. F, Pilbrow J. R, Ciccotosto G. D, Lau T. L, Tew D. J, Perez K, Wade J. D, Bush A. I, Drew S. C, Separovic F, Masters C. L, Cappai R, Barnham K. J. Copper-mediated amyloid-beta toxicity is associated with an intermolecular histidine bridge. J. Biol. Chem. 2006 Jun;281:15145-15154.

120. Cherny R. A, Atwood C. S, Xilinas M. E, Gray D. N, Jones W. D, McLean C. A, Barnham K. J, Volitakis I, Fraser F. W, Kim Y, Huang X, Goldstein L. E, Moir R. D, Lim J. T, Beyreuther K, Zheng H, Tanzi R. E, Masters C. L, Bush A. I. Treatment with a copper-zinc chelator markedly and rapidly inhibits beta-amyloid accumulation in Alzheimer's disease transgenic mice. Neuron. 2001 Mar;30:665-676.

121. Cuajungco M. P, Goldstein L. E, Nunomura A, Smith M. A, Lim J. T, Atwood C. S, Huang X, Farrag Y. W, Perry G, Bush A. I. Evidence that the beta-amyloid plaques of Alzheimer's disease represent the redox-silencing and entombment of abeta by zinc. J. Biol. Chem. 2000 Jun;275:19439-19442.

122. Faller P. Copper and zinc binding to amyloid-beta: coordination, dynamics, aggregation, reactivity and metal-ion transfer. CHEMBIOCHEM. 2009 Dec;10:2837-2845.

123. Rajendran R, Minqin R, Ynsa M. D, Casadesus G, Smith M. A, Perry G, Halliwell B, Watt F. A novel approach to the identification and quantitative elemental analysis of amyloid deposits--insights into the pathology of Alzheimer's disease. Bichem. Biophys. Res. Commun. 2009 Apr;382:91-95.

124. Lovell M. A, Robertson J. D, Teesdale W. J, Campbell J. L, Markesbery W. R. Copper, iron and zinc in Alzheimer's disease senile plaques. J. Neurol. Sci. 1998 Jun;158:47-52.

125. Talmard C, Guilloreau L, Coppel Y, Mazarguil H, Faller P. Amyloid-beta peptide forms monomeric complexes with Cu(II) and Zn(II) prior to aggregation. CHEMBIOCHEM. 2007 Jan;8:163-165.

126. Sitkiewicz E, Kłoniecki M, Poznański J, Bal W, Dadlez M. Factors influencing compact-extended structure equilibrium in oligomers of aβ1-40 peptide--an ion mobility mass spectrometry study. J. Mol. Biol. 2014 Jul;426:2871-2885.

127. Noy D. Solomonov I, Sinkevich O, Arad T, Kjaer K, Sagi I. Zinc-Amyloid β Interactions on a Millisecond Time-Scale Stabilize Non-fibrillar Alzheimer-Related Species. J. Am. Chem. Soc. 2008 Jan;130:1376-1383.

128. Yang M, Teplow D. B. Amyloid beta-protein monomer folding: free-energy surfaces reveal alloform-specific differences. J. Mol. Biol. 2008 Dec;384:450-464.

129. Walsh D. M, Lomakin A, Benedek G. B, Condron M. M, Teplow D. B. Amyloid beta-protein fibrillogenesis. Detection of a protofibrillar intermediate. J. Biol. Chem. 1997 Aug;272:22364-22372.

130. Bitan G, Kirkitadze M. D, Lomakin A, Vollers S. S, Benedek G. B, Teplow D. B. Amyloid beta -protein (Abeta) assembly: Abeta 40 and Abeta 42 oligomerize through distinct pathways. Proc. Natl. Acad. Sci. USA 2003 Jan;100:330-335.

131. Raffa D. F, Rauk A. Molecular Dynamics Study of the Beta Amyloid Peptide of Alzheimer's Disease and Its Divalent Copper Complexes. J. Phys. Chem. B. 2007 Mar;111:3789-3799.

132. Boopathi S, Kolandaivel P. Role of zinc and copper metal ions in amyloid β-peptides Aβ1–40 and Aβ1–42 aggregation. RSC Adv. 2014 Aug;4:38951-38965.

133. Dong M, Li H, Hu D, Zhao W, Zhu W, Ai H. Molecular Dynamics Study on the Inhibition Mechanisms of Drugs CQ1–3 for Alzheimer

Amyloid-β40 Aggregation Induced by Cu2+. ACS Chem. Neurosci. 2016 Feb;7:599-614.

134. Velez-Vega C, Escobedo F. A. Characterizing the Structural Behavior of Selected Aβ-42 Monomers with Different Solubilities. J. Phys. Chem. B. 2011 Apr;115:4900-4910.

135. Yang C, Li J, Li Y, Zhu X. The effect of solvents on the conformations of Amyloid β-peptide (1–42) studied by molecular dynamics simulation. J. Mol. Struct. (THEOCHEM) Jan;895:1-8.

136. Sgourakis N. G, Yan Y, McCallum S. A, Wang C, Garcia A. E. The Alzheimer's peptides Abeta40 and 42 adopt distinct conformations in water: a combined MD / NMR study. J. Mol. Biol. 2007 May;368:1448-1457.

137. Yan Y, Wang C. Abeta42 is more rigid than Abeta40 at the C terminus: implications for Abeta aggregation and toxicity. J. Mol. Biol. 2006 Dec;364:853-862.

138. Foloppe N, Hartmann B, Nilson L, MacKerell A. D. Intrinsic conformational energetics associated with the glycosyl torsion in DNA: a quantum mechanical study. Biophys. J. 2002 Mar;82:1554-1569.

139. Mantri Y, Fioroni M, Baik M-H. Computational study of the binding of CuII to Alzheimer's amyloid-beta peptide: do Abeta42 and Abeta40 bind copper in identical fashion? J. Biol. Inorg. Chem. 2008 Nov;13:1197-1204.